ELSEVIER

Surface Science Reports 28 (1997) 1–64

surface science reports

Charge-transfer induced particle emission in gas surface reactions

T. Greber [1]

Physik Institut der Universität Zürich, Winterthurerstr. 190, CH-8057 Zürich, Switzerland

Manuscript received in final form 6 March 1997

Abstract

Highly exothermic gas surface reactions may lead to the emission of electrons, ions and photons. These particles stem from the non-adiabatic de-excitation of a system in which charge is transferred between the surface and the adsorbate. The main concepts for chemisorptive particle emission are reviewed, as is its application for the recording of reaction kinetics and finally the information that it can provide on the dynamics of charge-transfer reactions at surfaces is examined.

Keywords: Non-adiabatic reactions; Exoemission; Chemiluminescence; Chemisorption; Molecular dynamics

1. Introduction

Charge-transfer as a concept for the rearrangement of electronic bonds is important for the understanding of chemical reactions. If the enthalpy ΔG that is released in a charge-transfer reaction is large compared to thermal energies $k_B T$, and the reaction time not too long compared to $\hbar/\Delta G$, such reactions may lead to the emission of particles. In heterogeneous gas surface reactions visible photons, electrons and ions may be detected, whose energies exceed thermal fluctuations $k_B T$ by orders of magnitude. The emission of such particles sheds light on the particular reaction pathways and gives a measure for the "effective temperature" in these reactions. It provides microscopic insight into friction and related mechanisms of energy dissipation.

In gas–solid reactions these phenomena have been known since the turn of the century but their detailed understanding was not attained as fast as for the photoelectric effect. This is mainly due to the more complicated nature of the particle emission process and, more importantly, due to the large variety of different effects leading to particle emission. In today's surface science, however, it is possible to prepare well-defined surfaces and therefore single effects may now be isolated and studied.

[1]Tel.: + 41 1 257 5744; fax: +41 1 257 5704; e-mail: greber@physik-rzu.unizh.ch.

0167-5729/97/$32.00 © 1997 Elsevier Science B.V. All rights reserved
PII S0167-5729(97)00005-8

The main purpose of this paper is to review the recent developments in the field of non-adiabatic (i.e. diabatic) gas/surface reactions leading to particle emission. It starts from the key 1979 paper of Nørskov et al. [1], who explained surface chemiluminescence in a correlation diagram picture borrowed from gas phase experiments.

The paper is organized in four parts. The introduction provides a historical overview and a general description of non-adiabatic reactions. In Section 2, the main concepts for non-adiabatic particle emission are outlined. In Section 3, studies of reaction kinetics are discussed and in Section 4, the recent developments concerning the dynamics of highly exothermic gas surface reactions are reported.

1.1. History

The first reports on non-adiabatic reactions that lead to the emission of particles is closely related to the first experiments on the photoeffect. While the photoeffect was explained in 1905 the understanding of phenomena that were related with particle emission in the course of non-adiabatic reactions was left to later generations where the experimental and theoretical concepts were further developed.

When Hertz observed the ignition of a light arc by the light of another light arc [2] it was realized that matter may be ionized by light. Soon after these first gas phase experiments it was found that solids may also be ionized by light [3] and that the photo-electrically induced voltage depends on the wavelength of the light but not on its intensity [4]. Around the same time the first experiments with cathode rays and radioactivity were performed. McLennan [5] observed the emission of negative corpuscles after the illumination of salts with cathode rays and postulated it to be "a kind of radioactivity". Although this is not the case, it is accepted as the first paper on dosimetry. At the time when Einstein [6] explained the photoelectric effect heuristically, it was also found that ionization may occur without light [7]. Thomson observed the emission of negative particles when a liquid alkali metal was exposed to small amounts of different gases. He first addressed the question of where the energy for the particle emission comes from. Given the second law of thermodynamics the observation of the effect at isothermal conditions ruled out the possibility that the energy stems from the heat bath of the solid. Thomson stated the energy to come "from some change in the state of the working substance". He did not, however, find a clear answer as to how the "continuous transformation of internal atomic energy into heat" could work. A few years later Haber and Just [8] studied with careful experiments the ionizing action of gases on alkali metals and alloys. They attributed the emission to the "transition of the metals to the oxides (hydroxides)" and stated that "on a molecular level this will be a turbulent process". In their later paper they performed experiments on "clean" surfaces that had been produced during the formation of a metal drop in a vacuum below 10^{-3} Torr [9]. Haber and Just finally concluded that the reaction of phosgene or bromine with KNa alloys leads to electron emission with yields of the order of about $5 \times 10^{-4} e^-$ per ClK unit formed. Furthermore, reactions of HgCs, HgLi and HgK alloys with phosgene and bromine would lead to negative ion emission. It was, however, recognized that such experiments with clean and highly reactive metals were difficult and that the influence of the "Oxidhaut" could not be neglected. Until the systematic investigations of Denisoff and Richardson [10] accurate gas phase experiments played an important role in the development of the concepts of non-adiabatic emission. The study of cold flames [11,12] and chemiluminescence in halogen–alkali gas phase reactions showed that the

reaction cross-sections considerably exceed those derived from atomic hard sphere radii and finally led to the celebrated "harpooning" mechanism of Polanyi and Magee [13,14].

After the second world war the increased need for detectors of radioactivity triggered studies of dark current phenomena as e.g. encountered in Geiger Müller counting tubes [15–18]. These "Kramer effects" are named after Kramer, who coined the term "exoemission" for emission induced by exothermic processes. Nevertheless, definite answers to the most fundamental questions on exoelectron emission were still lacking even 10 years after the famous 1956 Innsbruck conference on the subject [19].

The race to the moon generated, among other things, ultra high vacuum technology and today's surface science [20]. From the end of the 1960s, reports of studies on gas adsorption and related electron and light emission on clean metallic surface appeared, as e.g. the magnesium–oxygen reaction [21–23]. These experiments were the starting point for a better understanding of electron, ion and photon emission in gas–solid reactions and led to a quantitative understanding of dynamic processes at surfaces.

1.2. Non-adiabatic reactions at surfaces

The re-establishment of thermal equilibrium is driven by the requirement that the Gibbs free energy should be minimized. This requirement does not, however, dictate how and how fast this equilibrium is reached. The relaxation processes, i.e. routes by which a system de-excites and reaches equilibrium may be evaluated on ground state potential energy surfaces, where the system moves adiabatically, i.e. without jumps. This means that the electronic system satisfies the Born–Oppenheimer approximation, i.e. it is always in thermodynamic equilibrium with the nuclear coordinates. The concept of solving the equation of motion on potential energy surfaces may not always be adequate for the description of the thermalization process since tunneling or excitation on non-ground state potential energy surfaces may occur. As soon as the timescales (i.e. velocities) of the electronic and nuclear motions become comparable, the Born–Oppenheimer approximation may break down. Such situations are met when atoms become hot during a reaction or when the electron density is low, as is the case in all solid–vacuum interfaces. There are a large number of phenomena where the electronic system relaxes in *jumps*, i.e. in energy steps exceeding $k_B T$. These large excitations may lead to the emission of particles such as photons, electrons or ions. Gas phase reactions are a known example of non-adiabatic reactions [24]. On surfaces such reactions are more difficult to access experimentally and to describe theoretically because a quasi-continuum of states has to be taken into account. Fig. 1 illustrates a chemical reaction that may proceed adiabatically or non-adiabatically by means of two crossing potential energy surfaces. If the reaction proceeds fast enough there is a finite probability that the system remains in the initial symmetry configuration $(M + X)$, which does not correspond to the adiabatic ground state $(M^+ + X^-)$. The relaxation to the ground state then may be realized by the emission of a photon or by a decay without radiation, such as an Auger de-excitation. The detection and interpretation of these particles gives a measure for the degree of excitation and illuminates the reaction pathways taken towards equilibrium. A large class of such non-adiabatic relaxations are the luminescence "phenomena" where, as the name implies, light is emitted with a spectrum different from that of a black body. In luminescence the system is excited from thermodynamic equilibrium by various processes such as by light (photoluminescence), by electron beams (cathodoluminescence), by ionizing radiation (radiolumines-

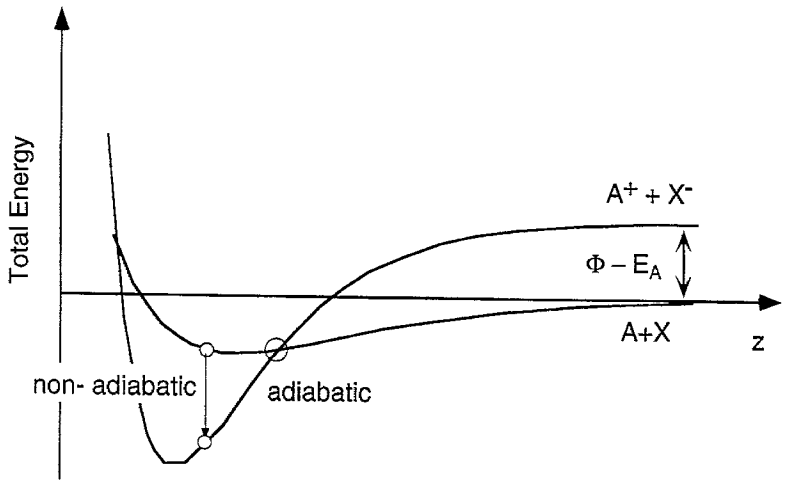

Fig. 1. Schematic potential energy diagram for a non-adiabatic charge-transfer reaction. A neutral adsorbate X approaches a surface A. When the two potential energy surfaces cross, adiabatic charge-transfer may occur. If the nuclear motion is fast, the charge-transfer may proceed via non-adiabatic de-excitation from $A + X$ to $A^+ + X^-$ with the emission of electrons or photons.

cence), by mechanical energy (triboluminescence), by biochemical energy (bioluminescence), by electrical energy (electroluminescence), by sound (sonoluminescence) or by chemical energy (chemiluminescence). In principle all these excitation schemes may also lead to de-excitation via the emission of electrons and ions. In this case the phenomena are labeled as *exoemission*. Following McKeever, the relaxation in luminescence is classified in terms of the typical time constant τ_0. Spontaneous processes, for which the relaxation occurs "instantaneously" with $\tau_0 < 10^{-8}$ s are called *fluorescent*. Stimulated relaxation processes with $\tau_0 > 10^{-8}$ s are called *phosphorescent* and, if 10^{10} y $> \tau_0 > 10^2$ s, *thermoluminescent* [25]. This classification can be adopted for exoemission phenomena as well, with the caveat that it is then misleading to speak of fluorescence and phosphorescence or thermoluminescence. It is more appropriate to distinguish between *spontaneous* and *stimulated* processes.

This review focuses on non-adiabatic particle emission by chemical reactions on solid surfaces. Related experiments as photon or electron stimulated desorption [73,74] or hyperthermal atom/ion scattering [135,136] are beyond the scope of this paper. The experiments discussed are performed on metallic surfaces where a continuum of low energy excitations such as e.g. electron–hole pairs are available. This means that luminescence phenomena are less prominent than in insulators or semiconductors, since more and faster de-excitation channels are available. Exoemission phenomena will dominate because electronic de-excitations are much faster than is the creation of light quanta. It must, however, be noted that the gas–solid interface also has the potential for "slow" electronic de-excitations as for luminescence, since the density of states and therefore the phase space, or the number of possible excitations, decreases on passing from the solid to the vacuum. This also leads to the possibility of ion escape from a surface reaction in which the escaping negative ion has a lower ionization potential than the work function of the surface [26].

The excitation of the system is the chemically induced energy that is released upon chemisorption of reactive gases. Spontaneous as well as stimulated non-adiabatic particle emissions can be observed. Spontaneous exoelectron emission is e.g. observed in the first stage of the oxidation of alkali metals where oxygen dissociates without any activation barrier [27], while the exoemission in the late stage of oxidation of alkali metals can e.g. be stimulated by thermal activation [28]. The stimulated processes are well suited to the study of the response of a system upon thermal or chemical stimulation. Kinetic analyses give hints as to the reaction pathway. It is, however, not straightforward to deduce a single microscopic model from the kinetics alone since these are a macroscopic description of an observed reaction. But kinetics allows one to falsify or rule out certain mechanisms. This ability often helps to unravel the puzzle of a reaction and should not be underestimated. The spontaneous processes on the other hand give more direct insight into the dynamics of the charge-transfer processes. Kinetic restrictions can be neglected in this case, and dynamical models with a microscopic description can be made compatible with electronic excitability and lifetimes. They give an estimate of the microscopic reaction time and of the intermediate velocities. These models can be tested more rigorously if the reactions are run under different "artificial" conditions. Such extra parameters are valuable to experimentally probe the reaction dynamics. A particularly interesting experiment was recently performed by using a seeded molecular beam in order to vary the impact velocity of molecules on surfaces [29], and velocities of reaction intermediates were determined from such experiments [30].

2. Theoretical concepts for chemisorption induced particle emission

Useful though a phenomenological description of non-adiabatic particle emission is, additional theoretical concepts that offer insight into the microscopic mechanisms of charge-transfer reactions are vitally important.

Theories for adiabatic gas surface reactions are well developed. For example the adsorption of hydrogen can be predicted quantitatively from six-dimensional potential energy surfaces that take the zero point energy into account [31,32]. It turns out that properties such as the velocity dependence of the sticking coefficient are fully described by the quantum mechanical motion of hydrogen on adiabatic ground state potential surfaces, and no energy dissipation has to be taken into account. This is not the case for non-adiabatic gas surface reactions where charge-transfer is an essential ingredient of the adsorption process. Therefore no single potential energy surface is able to describe the processes and correspondingly the theory for a complete picture must be more involved.

The phenomenon of non-adiabatic particle emission covers probabilities from 10^{-2} down to the detection limit of typically 10^{-12} particles per charge-transfer where photons, electrons and ions are found. The theories developed so far achieve a qualitative description in which the order of magnitude of the effects may be estimated [1,137,138] or in which reaction parameters may be extracted phenomenologically [30,33]. Multiple potential energy surfaces have been constructed in order to describe charge-transfer dynamics [34–138,139,140].

This section starts from Nørskov, Newns and Lundqvist model [1] for the chemiluminescence of alkali metal–halogen reactions and recalls the basic concepts for negative particle emission. Particular emphasis is placed on the spatial dependence of the timescales for motion in the electronic and nuclear subsystems, in order to rationalize negative ion emission. Finally the branching ratio

between photon and electron emission is discussed in Section 2.3 and it is shown how this quantity is a measure of the electron density at the site of de-excitation.

It is not the intention here to give an account of the theories that were developed in the context of non-adiabatic particle emission from insulators, such as the chemiluminescence from F-center de-excitations in MgO [39–41].

2.1. Chemiluminescence

The reverse process to photo dissociation, i.e. radiative recombination of atoms, may also occur in a reaction. The reaction rates are, however, expected to be small since the radiative lifetime of electronic transitions (~ 10 ns) exceeds that of typical collision times (~ 100 fs) by about five orders of magnitude [41].

Fig. 2 shows the simplest form of correlation diagram that depicts a chemiluminescent reaction between an alkali atom A and a halogen atom X. For simplicity, only the highest unoccupied (HUMO) and the lowest unoccupied (LUMO) molecular orbitals are shown. At the beginning of the reaction the valence electron sits on the alkali atom s orbital with even symmetry. The hole in the halogen p valence shell forms the affinity level with odd symmetry. The energy difference between the two levels corresponds to the difference between the ionization potential of the alkali atom and the electron affinity of the halogen atom, respectively. When the two reactants approach each other the energies of the two orbitals cross and the AX dimer arrives in an excited state AX^* with even symmetry. From this state the system may scatter back $AX^* \rightarrow A + X$ or de-excite via electron transfer into the halogen derived p hole inducing chemiluminescence $AX^* \rightarrow AX + \hbar\omega$. This reaction path is non-adiabatic since the systems does not follow the lowest possible energy state in the correlation diagram.

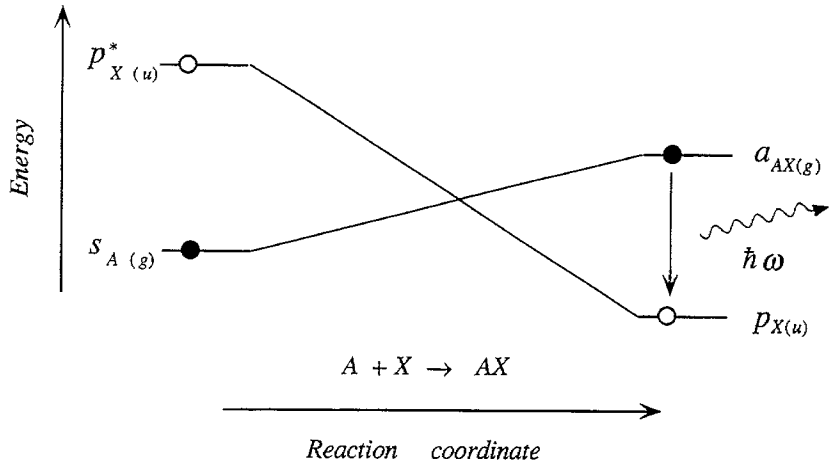

Fig. 2. Correlation diagram for the reaction of an alkali atom A with a halogen atom X ($A + X \rightarrow AX$). The energy of the lowest unoccupied molecular orbital (LUMO) of X and the highest occupied molecular orbital (HOMO) of A are shown along the reaction coordinate, as is the internuclear spacing. The two levels may cross and the charge-transfer from the A derived level into the X p-level may proceed under the emission of a photon that restores the p symmetry of the AX ground state.

Nørskov et al. [1] addressed for the first time the role of the solid, in which the situation is more complicated and where the symmetry arguments are not as rigorous as in the case of the two body problem, since the solid provides a quasi-continuum of states. They nevertheless arrived at a quantitative description for the experimentally observed chemiluminescence spectra from the reaction of sodium with I_2, Br_2 and Cl_2 [43]. Later, this picture was consistently applied by Andersson et al. [44] to the case of Cl_2 on potassium. The picture drawn from the theoretical model was that the halogen molecules X_2 get harpooned $X_2 \rightarrow X_2^-$ at a relatively large distance from the surface and that dissociation $X_2^- \rightarrow X^- + X^*$ starts. Finally the neutral halogen X^* may de-excite in front of the surface via charge-transfer induced emission of a light quantum $X^* \rightarrow X^- + \hbar\omega$. It is known from gas phase experiments [14,45] that the harpooning distance $z_{\text{harpooning}}$ is not determined by the image potential of the adiabatic affinity of the molecule, but by that of the vertical affinity E_A^V which is the affinity at the internuclear spacing of the neutral molecule. The potentials for Cl_2, Cl_2^- [46] and O_2, O_2^- [47] are shown in Fig. 3. While there is still a positive vertical electron affinity in the case of Cl_2, this affinity is negative for O_2.

The harpooning distance $z_{\text{harpooning}}$ from the image plane for $\Phi > E_A$ becomes:

$$z_{\text{harpooning}} = \frac{e^2}{4\pi\varepsilon_0} \frac{1}{4(\Phi - E_A^V(X_2))} = \frac{3.6\,\text{Å}}{\Delta E\,(\text{eV})}. \tag{1}$$

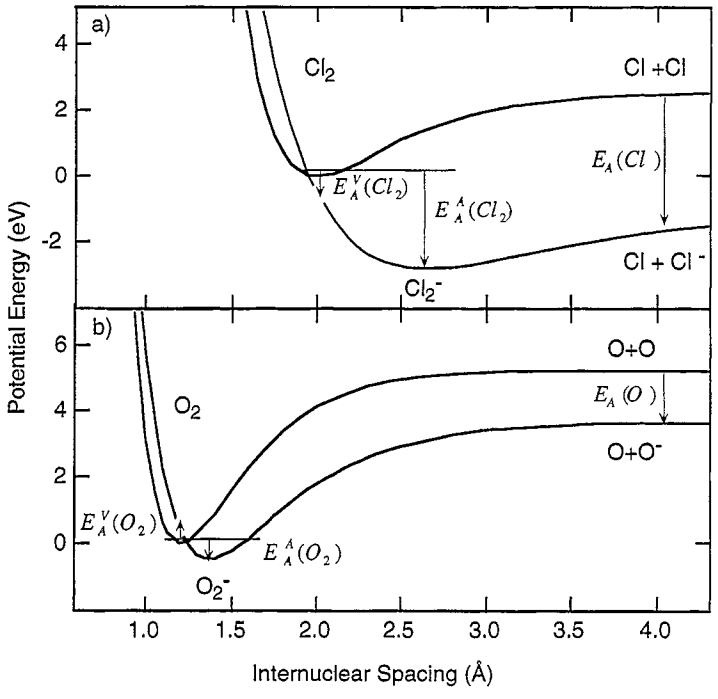

Fig. 3. Potential energy curves (a) for Cl_2 and Cl_2^- from [46] and (b) for O_2 and O_2^- from [47] as a function of the internuclear distance. The difference between the adiabatic E_A^A and the vertical electron affinity E_A^V is clear from this figure. The vertical electron affinity determines the harpooning distance.

Up to the image potential induced factor of 4 this is the same formula as that for the gas phase reactions formulated by Magee [14]. From Eq. (1) it can be seen that the harpooning occurs closer to the surface for large $\Delta E = \Phi - E_A^V(X_2)$ and that the Coulomb force F_C at the harpooning distance $z_{\text{harpooning}}$ becomes:

$$F_C(z_{\text{harpooning}}) = \frac{4\pi\varepsilon_0}{e^2} 4(\Phi - E_A^V(X_2))^2 = \frac{e^2}{4\pi\varepsilon_0}\left(\frac{1}{2z_{\text{harpooning}}}\right)^2. \tag{2}$$

The Coulomb acceleration that occurs after a charge-transfer is therefore largest for large ΔE values and exceeds that of gas phase reactions by the image force induced factor of 4. This holds as long as the image acceleration dominates the Pauli repulsion that will set in at electron densities above that of bulk Li [48].

The spectrum of chemiluminescence is an important fingerprint for the encoding of non-adiabatic reactions. In contrast to gas phase reactions, broad spectra [23,40,43] and only weak narrow gas phase lines have been observed [49]. From a model that describes the probability $P_h(\varepsilon_x)$ of a hole state at energy $\varepsilon_x(t)$ and the decay $\Gamma_{\text{Photon}}(\hbar\omega,\varepsilon_x)$ into a photon of energy $\hbar\omega$, the emission spectrum is found by the folding of these two entities [1]:

$$P_{\text{Photon}}(\hbar\omega) = \int P_h(\varepsilon_x,t)\Gamma_{\text{Photon}}(\hbar\omega,\varepsilon_x)\mathrm{d}t. \tag{3}$$

For spontaneous emission, $\Gamma_{\text{Photon}}(\hbar\omega,\varepsilon_x)$ is proportional to ω^3 [50] and for a continuum of final states we find a continuous spectrum with a cut off at the maximum excitation energy ε_A.

Together with a description of the decay probability of a neutral halogen atom in front of a metallic surface, $P_h(\varepsilon_x)$, this theory reproduced the observed chemiluminescence spectra in the reaction of Cl_2, Br_2 and I_2 with sodium surfaces [43]. Although the issue of vertical affinity was neglected in the original paper of Nørskov et al. [1] it does not affect the calculated chemiluminescence spectra significantly since these spectra are independent of whether the chemiluminescence reaction takes place on an outgoing or impinging trajectory of the ballistic X^* atoms.

In the case of the reaction of oxygen with Li, no chemiluminescence was found [51]. This can be understood since the charge-transfer on the O_2 molecule occurs much closer to the surface than for the halogen molecule and so it is more likely that the de-excitation occurs via electron–hole pair creation or by exoelectron emission. Total energy calculations indicated the charge-transfer that leads to exoelectron emission below the surface [27]. The comparison between electron emission ($10^{-8}e^-/O_2$) and the negligible visible photon emission ($< 10^{-11}/O_2$) shows that in this case the de-excitation process is indeed much more efficient on dark paths [33].

2.2. Negative particles

While the reaction of two atoms may proceed chemiluminescently, there exists one reaction, uranium with oxygen, in which two atom associative electron detachment $A + B \rightarrow AB^+ + e^-$ has been observed at thermal energies [52]. Ion separation $A + B \rightarrow A^+ + B^-$ is forbidden since all these reactions are endoergic, i.e. the ionization energy exceeds the electron affinity for all elements. In going to reactions with alkali dimers A_2 and halogen molecules X_2 ionization reactions of the type

$A_2 + X_2 \rightarrow A^+ + AX + X^-$; $A_2X^+ + X^-$; $A^+ + AX_2^-$ were observed [53,54]. For the case of A_2 and X_2 the molecular bond may be broken by an e^- jump from the A_2 on the X_2 molecule. Now the non-adiabaticity that strongly depends on the geometrical orientation of the reacting molecules may preserve the charged state of the products that do not represent the lowest energy state.

This section briefly reviews the basic concepts of the work function since this is important for the emission of electrons, and also, in combination with the electron affinity, for the emission of the negative ions. X^- emission is expected in an $M + X_2$ reaction if the work function Φ of the metal M is smaller than the electron affinity of the emitted atom $E_A(X)$ [55,56]. Recently it was found that this "downhill" condition $\Phi(M) < E_A(X)$ must not necessarily be fulfilled. If X^- is formed in the course of the reaction and if its velocity is large enough, an ion can escape from a surface and the jump back of the electron from the ion into the Fermi sea may be skipped [26].

The probability of an Auger de-excitation leading to the emission of an exoelectron [21,33,56–59] is discussed in Section 2.2.3. It is shown there that this much faster de-excitation channel is more likely than chemiluminescence to occur in gas–solid reactions.

2.2.1. The role of the work function

To describe the energies of emitted negative particles an appropriate energy reference must be chosen. Fig. 4 illustrates the three points of reference that come into play in a one particle picture that describes an electron in an effective potential which is given by the rest of the system: (i) the vacuum level E_V, which is the kinetic energy zero point for particles in the vacuum, (ii) the Fermi level or chemical potential E_F, which is the zero point for excitations in the solid, (iii) the valence band bottom E_0, which is the kinetic energy zero point for particles in the valence band. In this paper the energies labeled with the latin letter E increase in going from E_0 to E_V. On the other hand excitation energies labeled with the greek letter ε increase in going from E_F to E_0.

The energy difference between the vacuum level and the valence band bottom is referred to as the inner potential $U = E_V - E_0$ and that between the vacuum level and the Fermi energy as the work function $\Phi = E_V - E_F$ [60]. The latter is the minimum energy required to remove an electron from the solid while an N particle system is transformed into an $N - 1$ particle system. Exceptions to this rule, which is founded on energy conservation and the Pauli principle, may be expected if electrons

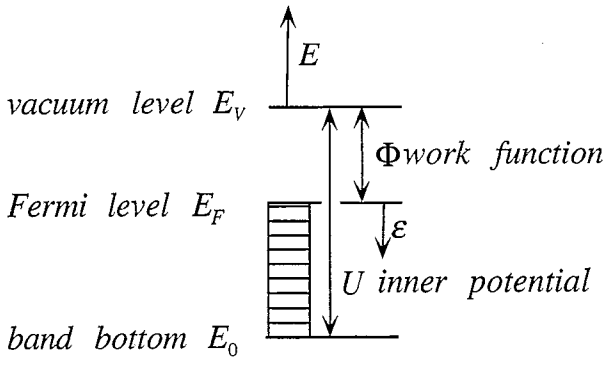

Fig. 4. Scheme for the energy reference points as described in the text.

remain excited in metastable states above the Fermi level. Such situations are observed in optically stimulated exoelectron emission (OSEE) where for example photoemission from color centers in an ionic crystal may lead to emission below the photo threshold of the solid [61]. The work function is also closely related to the electron affinity of a metal, defined as the energy difference between the N and the $N+1$ particle system.

It is important to address the question of how the yield depends on the excitation energy. For photoelectron emission from metals this led to the famous Fowler law [62], which states that the photoelectric yield close to the threshold is proportional to the square of the maximum photoelectron energy in the vacuum $Y \propto (\hbar\omega - \Phi)^2$. Here the photon energy corresponds to the excitation energy and the work function acts as the emission threshold. Such a power law was encountered in numerous experiments, but, the value of the exponent was found to deviate from 2 [63, 64].

The work function strongly affects the emission of negative particles in non-adiabatic reactions since the maximum available free enthalpy per charge transfer is of the order of the work function. For small excess energies E_x, $E_x/\Phi \ll 1$ the dependence of the yield on the excitation ε_x in a system with work function Φ can also be described by a power of the excess energy measured with respect to the vacuum level $E_x = \varepsilon_x - \Phi$. Therefore, we expect a yield dependence $Y \propto E_x^{\kappa}$, where κ depends on the excitation process. In the simplest model the yield will depend on the convolution of the escape function (i.e. the emission probability) with the kinetic energy spectrum in the solid. The escape function must take the refraction and the source wave character of the electrons into account. This fact was not considered by Fowler [62].

Refraction conserves parallel momentum while normal momentum $\hbar k_\perp$ pays for the inner potential that is overcome in the emission process. Inside the solid this limits the cone of possible emissions to that of electrons with $(\hbar^2/2m)\, k_{i\perp}^2 > U$, where U is the inner potential $E_V - E_0$.

For an isotropic electron source wave this leads a total yield proportional to the solid angle of the total reflection cone $\tan(\theta_c) = \sqrt{E_m/U}$, where E_m is the measured kinetic energy with respect to the vacuum level and θ_c is the half angle of the total reflection cone. For $E_m \ll U$ and isotropic emission, the yield is proportional to the momentum of the electrons in the vacuum, $Y = \frac{1}{2}\sqrt{E_m/U}$ [65,66].

For isotropic emission the angular distribution $P_e(\theta)$ as a function of the polar emission angle θ measured from the surface normal thus becomes

$$P_e(\theta) = \sqrt{\frac{\cos(\theta)^2}{\cos(\theta)^2 + U/E_m}}, \tag{4}$$

where for $E_m \ll U$ the electron emission follows a $\cos(\theta)$ law. Note that this $\cos(\theta)$ dependence does not have the same origin as that in Lambert's law.

The kinetic energy spectrum will depend on the excitation and de-excitation. If this spectrum is a delta function $\delta(E_m - E_x)$ a yield proportional to $\sqrt{E_x}$ would follow from the above. This is, however, a hypothetical case. In Fig. 5 a more realistic scenario is shown for the Auger de-excitation of a hole state at ε_x below the Fermi level E_F. Without refraction a linear kinetic energy spectrum $S(E_m) \propto (E_x - E_m)$ and $S = 0$ for $E_m > E_x$ is expected. This linear dependence assumes a constant matrix element and density of states for all de-excitations in the energy interval $E_x \geq E_m \geq E_V$ [33].

Solving the convolution integral of the escape function with the linear kinetic energy distribution gives a yield dependence $Y \propto E_x^{5/2}$ and indicates a strong dependence of the exoelectron emission on the work function [33]. For the description of a dynamical process such as injection of a hole into an

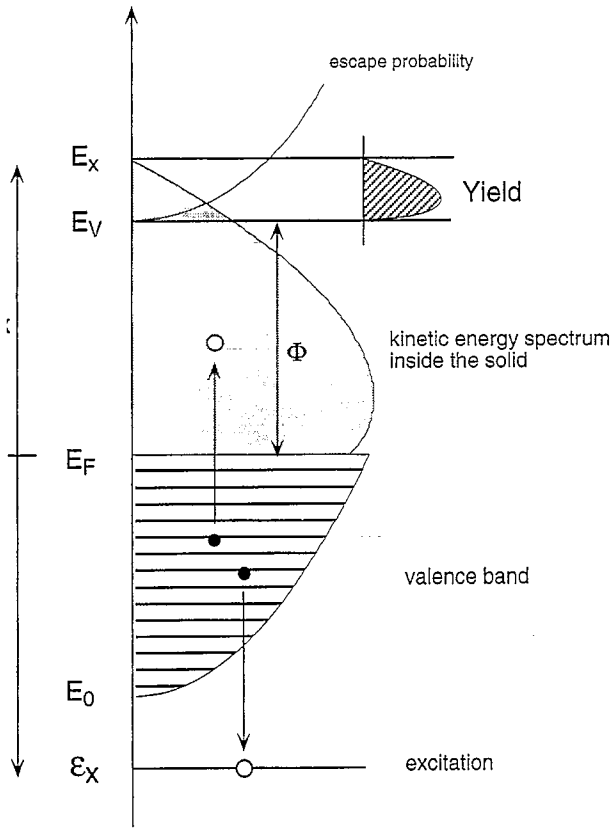

Fig. 5. Auger de-excitation of a hole state in the valence band. On convolution of the kinetic energy spectrum in the solid with the escape function the yield becomes proportional to $E_x^{5/2}$, where $E_x = \varepsilon_x - \Phi$ is the excess energy.

electron gas, where the excitation is not created suddenly at ε_x, the exponent is expected to be larger than 5/2 since the hole may decay during the injection.

2.2.2. *Ion emission*

Negative ion emission from gas surface reactions was pioneered by Trowbridge and Herschbach [55] and by Prince and coworkers [56,67,68]. They found X^- halogen ion emission in the reaction of X_2 halogen molecules with low work function surfaces. The understanding of these phenomena has profited from related work, i.e. negative ion production, neutralization and scattering at intermediate energies as is encountered for example in sputtering or ion scattering [69–72].

The escape of a negative ion from a gas surface reaction is an indication of non-equilibrium conditions during the reaction. In order to drive such processes, electronic energy has to be transferred into nuclear motion directed away from the surface. Much can be learnt from the observation of negative ions by invoking energy and momentum conservation.

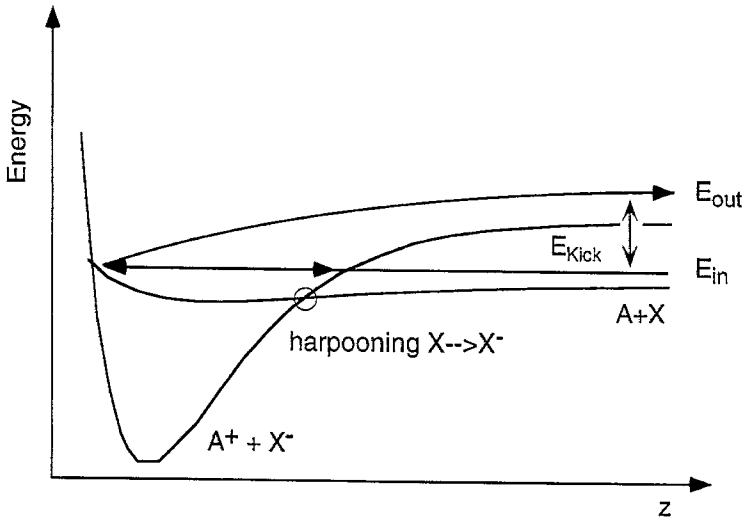

Fig. 6. Two potential energy surfaces $A + X$ and $A^+ + X^-$ for neutral and charged adsorbates X and X^-, respectively, as a function of the distance z from the surface. A harpooned particle may leave the surface only if additional kinetic energy E_{Kick} is transferred to the ion. Otherwise the ion gets trapped by its image potential or has to reneutralize for backscattering.

First, the overall reaction has to be exothermic and secondly, momentum has to be transferred to the back scattering ion. It is important to note that the momentum transfer from elastic scattering is not sufficient for the production of free negative ions since an ion tends to be trapped by its image potential. Therefore a mechanism that transfers energy into translational energy of the outgoing ion must be at work. The kick to the outgoing ion may stem from the transformation of vibrational energy or from the momentum of the dissociation partner. In Fig. 6 the most general scenario is sketched: As soon as a molecule approaching a surface gets resonantly ionized (harpooned) it accelerates in the image field. If the ion scatters elastically it may not escape the image potential anymore: It will scatter back to the harpooning distance, where it is still trapped by its image potential and where it is expected to dissipate its kinetic energy and to rest on the surface. If, however, the ion gets momentum from the electron jump it may be kicked off the surface. Since the momentum of the electron is too small for this task a mechanism that transforms the change in electronic structure into nuclear motion has to operate. This furthermore emphasizes that two one-dimensional potential energy surfaces, as shown in Fig. 6, are not sufficient to describe the process. Additional kinetic energy has to couple to the translational motion of the ion. Models for such mechanisms are well developed e.g. for the case of photo stimulated desorption [73], or electron stimulated desorption [74] where the excited species accelerates during its lifetime towards the equilibrium coordinates of the excited system and eventually picks up enough momentum for desorption.

Two classes of negative ion emission reactions have to be distinguished: (i) non-dissociative and (ii) dissociative negative ion escape.

(i) The only known example for the first class is that of NO_2^- emission from Cs surfaces. Fig. 7 shows the negative particle emission upon the reaction of one monolayer of Cs on Ru(0 0 0 1) with

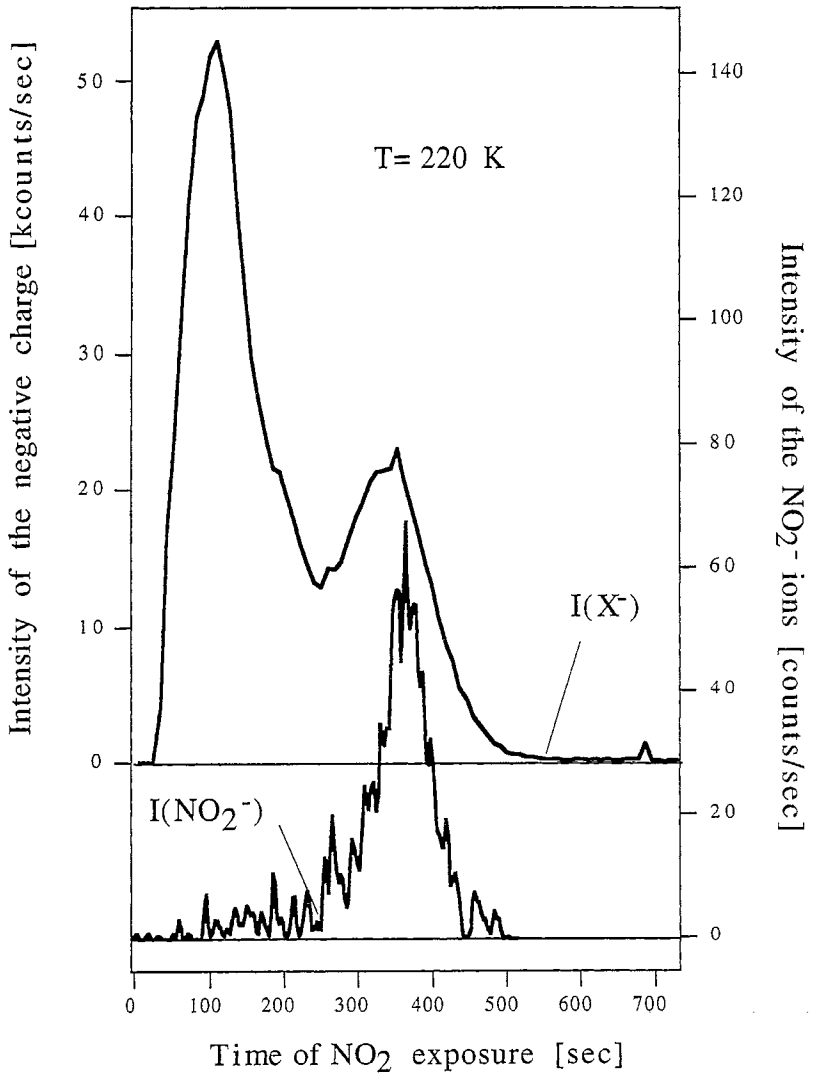

Fig. 7. Negative particle emission from the oxidation of one monolayer of Cs on Ru (0001) with NO_2. The exposure is normalized with the exposure to the work function minimum. The emission at the work function minimum comprises ions of mass 46. From [75].

NO_2, as a function of the gas exposure [75]. In the later stage of the reaction, when the surface passes its work function minimum, the negative particles were identified as NO_2^- ions. Apparently, a single electron transfer is sufficient for the back scattering of negative ions. In order to conserve energy the adiabatic affinity E_A^A has to exceed the work function. The exothermicity is E_A^A $(NO_2) - \Phi$, in this case (0.6 eV). This energy release does not correspond to the largest enthalpy for this reaction since the energy of an ion close to a metallic surface is additionally lowered by the image and the physisorption potentials. The physisorption potential results from the image force of dipole

fluctuations and is much weaker than the image potential of an ion. The ion has to get kinetic energy that pays for the escape from the image potential at the harpooning distance (cf. Eq. (1)). If no momentum but that of the elastic scattering were transferred to the NO_2^- ion, harpooning would have to be taking place for image potentials comparable with $k_B T$. This corresponds to a distance of about 140 Å for room temperature molecules (cf. Eq (1)). It is unlikely that electrons from the substrate will tunnel out this far in order to ionize an approaching molecule. Harpooning occurs closer to the surface and therefore a mechanism has to provide momentum for the surmounting of the image potential at the harpooning distance. A cold surface provides no excess momentum. It has therefore to stem from the release of internal energy that is liberated due to the relaxation of the harpooned molecule into the equilibrium coordinates of the negative ion. For example the NO_2 molecule is bent as an isosceles with an angle of 120° between the N–O bonds [76], which transforms upon harpooning to about 90°. Therefore it is obvious that the ν_2 scissors vibration (80 meV) will be excited from the relaxation energy in the $NO_2 \xrightarrow{+e^-} NO_2^-$ reaction. This relaxation energy corresponds to the difference between the vertical affinity E_A^V and the adiabatic affinity E_A^A (see Fig. 3). If we assume that the ion scatters elastically from the surface, vibrational energy has to be transformed into translational energy, in a kind of anti-Stokes process to allow negative ion escape from the image potential. From these considerations it becomes clear that no direct negative (and positive) ion back scattering is expected for atomic scattering since no relaxation energy is available, i.e. E_A^V and E_A^A are equal. The relaxation energy $E_A^A - E_A^V$ is crucial for the understanding of the dynamics of negative ion formation. If the relaxation energy may not exceed the heat of formation $E_A^A - \Phi$, then the even stronger condition $E_A^V > \Phi$ applies if ionic emission without dissociation is to be possible.

(ii) If dissociation of the molecules is involved in negative ion emission, the situation becomes more complex. The energy condition $E_A^V > \Phi$ derived above no longer holds since the heat of formation of the molecular fragments that remain on the surface has to be included in the energy balance. This was shown experimentally by the observation of O^- emerging from the reaction of O_2 with Cs [26]. In this case the work function of the surface is larger than the electron affinity of oxygen. This "uphill" reaction ($E_A < \Phi$) demonstrates that the oxygen ion must get a large momentum contribution (exceeding $\sqrt{k_B T m}$) from the process in order to escape the surface. This must come from the reaction enthalpy of the oxygen atom remaining on the surface. Indeed, the reaction of $4Cs + O_2 \xrightarrow{+e^-} 2Cs + Cs_2O + O^-$ is exothermic by about 0.1 eV. As can be seen, three electron transfers are involved in the reaction in this case. Correspondingly, the description of the reaction is more complex than if only one electron is transferred, as for example in the case of $Cs + NO_2 \xrightarrow{+e^-} Cs + NO_2^-$. An intermediate situation is the reaction of halogens X_2 with alkali metals in which the first electron transfer may lead to dissociation and where negative ion emission is observed [37,55,56]. Although these reactions fulfill the downhill condition $\Phi < E_A(X)$ a large transfer of momentum must occur to the X^- ion. To be more specific let us consider the reaction $K + Cl_2$ (cf. Fig. 3). Here the vertical affinity $E_A^V(Cl_2) = 1.0$ eV is smaller than the work function of K (2.3 eV) and the image potential at the harpooning distance (1.3 eV) has to be overcome for Cl^- escape. Since the harpooned Cl_2^- starts to dissociate spontaneously it is more appropriate to talk of momentum transfer from the remaining Cl atom to the back scattering Cl^- ion. A one-dimensional hard sphere model shows the momentum to increase by a factor of 2 if all the momentum of the remaining Cl atom is transferred to the Cl^-. If the Cl_2^- is accelerated to more than 1.3 eV kinetic

energy at the point of dissociation, such a kick is sufficient for the escape of the Cl^- ion from the image potential at the harpooning distance $z_{harpooning}$. For the case of $K + Cl_2$ an integration of the equation of motion shows that a time of about 150 fs is needed for the acceleration of Cl_2^- to 1.3 eV kinetic energy. This 150 fs corresponds to 1.2 vibrational periods [77] and it is therefore a plausible mechanism for the observed Cl^- emission from alkali metal surfaces [55].

The above considerations show that the orientation of the ions at the point of dissociation is important in order to gain enough momentum normal to the surface. It has furthermore to be noted that in dissociative negative ion reactions it is likely that neutral atoms are scattered off the surface as well. This is particularly true for the case of the $Cs + O_2$ reaction where the system gains energy if the electron on the escaping oxygen atom tunnels back into the Fermi sea of the substrate.

For such processes it is possible to measure not only the energy and momentum, but also the probability that they will occur. For the case of dissociative negative ion back scattering the probability of a negative ion per incoming molecule P_{ion} follows the trend $P_{ion} = p_0 \exp((E_A - \Phi)/k_B T_{eff})$. From the data of the halogen + alkali metal experiment of Trowbridge and Herschbach [55] and those from oxygen + alkali metals [26,51], $k_B T_{eff} = 0.15$ eV and $p_0 = 10^{-7}$ fit the data best. Fig. 8 shows the correlation between $\log(P_{ion})$ and $\Phi - E_A$. The value for the slope $1/k_B T_{eff}$ is clearly smaller than $1/k_B T$ and may be attributed to an effective temperature of about 1800 K. The factor p_0 is small and indicates a fairly low overall probability of ionic back scattering.

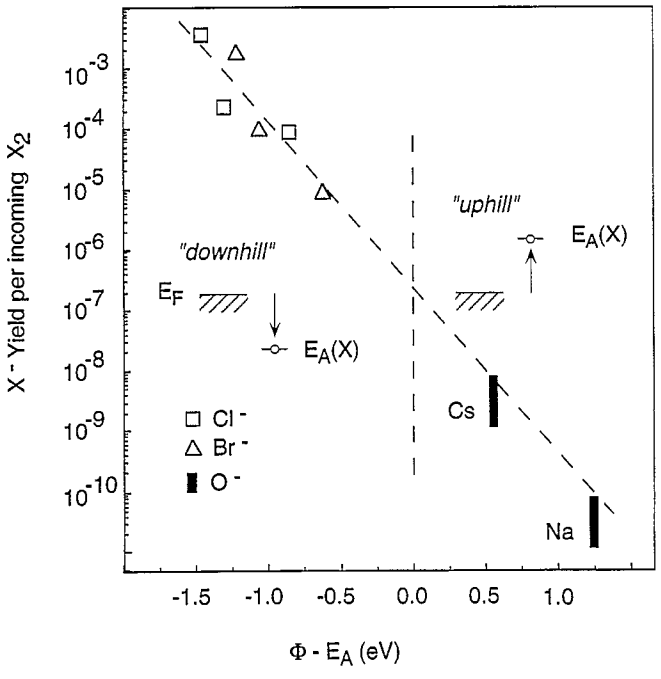

Fig. 8. Logarithmic plot of chemical ionization yields from surfaces versus the energy difference of the work function and the affinity level of the escaping atomic species. The open symbols are values taken from [55], and the dashed line is the exponential trend from these values. This trend, proportional to $\exp(-\Delta E/k_B T_{eff})$ ($k_B T_{eff} = 0.16$eV) continues for "uphill" reactions ($\Phi > E_A$), as is indicated with the initial emission probabilities in the O_2 on Cs and O_2 on Na reactions. From [26].

Apparently the phase space that allows ionic back scattering is small compared to all other reaction pathways. This suggests again that the geometric orientation of the scattering molecules is important in this kind of reaction.

For a more quantitative understanding of negative ion emission the lifetimes of the involved states and the charge-transfer mechanism must also be considered. In particular the timescales for nuclear motion and electronic motion must be compared. Fig. 9 sketches the basic mechanism that is involved in an ion emission reaction: $AX^- \rightarrow A^- + X$ or $A + X^-$. It is depicted as a double well potential where the ground state wave function for the lowest bound electron has a component centered on A and a component centered on X. If the reaction provides enough momentum transfer, the two species may be separated so fast that there remains a finite probability for the electron to stay "frozen" on the X^- ion, even if this does not correspond to the adiabatic ground state. At the freezing point the electronic and nuclear velocities will be of the same order of magnitude and the Born–Oppenheimer approximation breaks down.

Kimmel and Cooper [72] treat the two timescales of nuclear and electronic motion within a one-dimensional one particle model. The model comprises a continuum of electronic states of a jellium-like substrate and an adsorbate that is described by the affinity level with a z-dependent energy ε_A and width Δ. The timescale for electronic motion is related to the lifetime of the adsorbate level or hybridization Δ between the adsorbate affinity and the solid. The hybridization is commonly

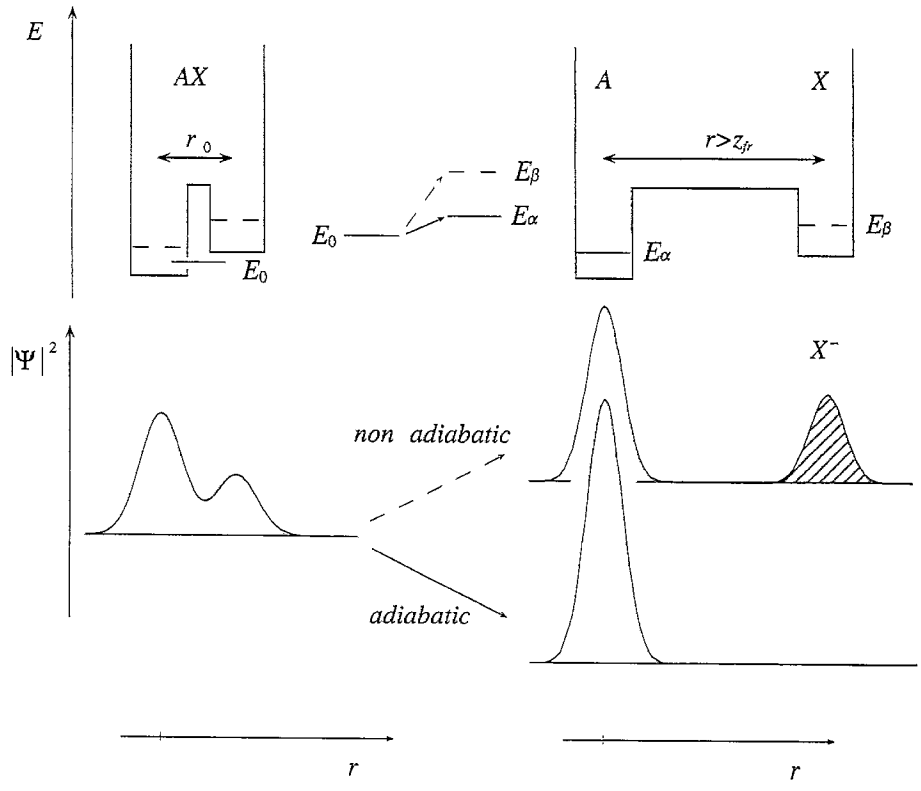

Fig. 9. Schematic diagram that depicts the possibility of negative ion desorption for atomic species X with smaller electron affinities than the work function. In the top panel the energy diagram and in the bottom panel the wave function of the lowest unoccupied orbital (LUMO) is shown for the adsorbed AX and the desorbed/dissociated $A + X$ configuration. If the dissociation is fast enough there is a finite probability that the electron gets frozen in the energetically unfavorable ionic state $A^+ + X^-$.

assumed to decay as $\Delta(z) = \Delta_0 \exp(-z/l_0)$, where l_0 is a measure of the leaking out of the electrons into the vacuum [78]. Although this may describe the observed trends, it is nevertheless not universally applicable [79]. In this description the hopping time τ_e for the electrons between the solid and the adsorbate becomes $\tau_e = h/2\Delta$, where Δ depends on ε_A and on the distance z to the surface. Values for Δ_0 and l_0 can be determined from calculations. Taking calculations from Nordlander and Tully [79], for example, for aluminium with a Wigner–Seitz radius $r_s = 2$ Bohr radii a_0 in the range of $z = 10 \pm 3\ a_0$ for the Li 2s level, we find a value of 210 eV for Δ_0 and of 0.55 Å for l_0. In the results illustrated in Fig. 10 the parametrization of Kimmel and Cooper was adopted to take into account the Pauli repulsion induced saturation of the lifetime at high electron densities Δ_{sat} of about 1 eV [72]. The second timescale $\tau_{nuc} = l_0/v_\perp$ is given by the nuclear motion, where l_0 is the length scale of the electronic lifetime and $v_\perp$ is the normal velocity of the nucleus. In the case of ion scattering with primary energies between 5 and 1000 eV, τ_{nuc} is considered to be constant, and no memory of the incoming trajectory was observed experimentally [72]. For lower impact energies such as we encounter in the case of the reactive scattering of thermal molecules we expect that the image acceleration and in particular the harpooning distance should influence the incoming trajectory. The nuclear timescale therefore becomes $\tau_{nuc} = l_0/v_\perp(z)$, where $v_\perp(z)$ is mainly determined by the image potential at the harpooning distance. When the electronic timescale is equal to the nuclear timescale on the outgoing trajectory the charge state will freeze at z_{fr}. For $z > z_{fr}$ the nuclear motion is larger than the electronic motion that would allow a charge-transfer. Thus the degree of occupation of the affinity level at z_{fr} determines the average ionicity of the outgoing atom. This has implications for the

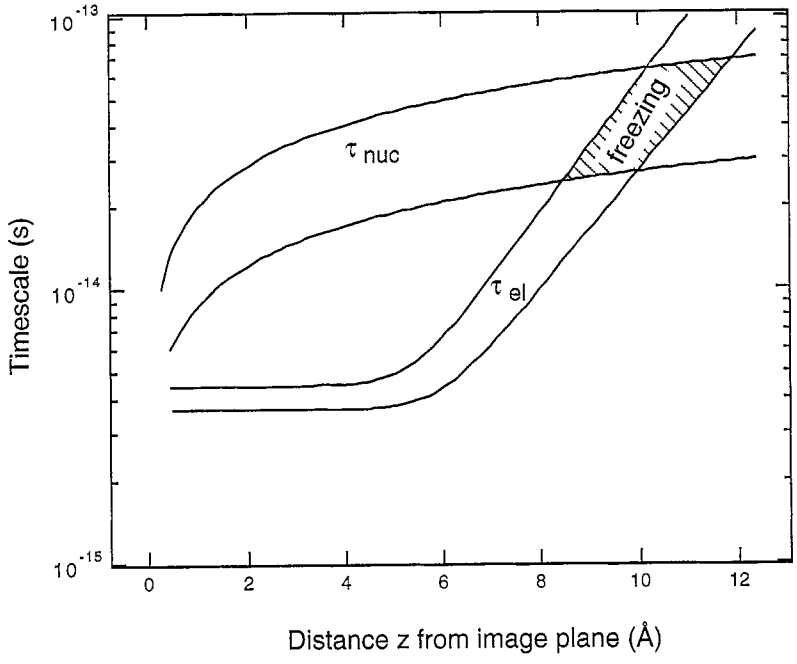

Fig. 10. Timescales for the nuclear τ_{nuc} and the electronic τ_{el} motion close to a surface as a function of distance from the surface. For definition see text. When these timescales are equal, the electronic state gets frozen on a desorbing nucleus. It can be seen that the velocity of the nucleus strongly influences the freezing distance.

interpretation of ion emission, as was pointed out for example by Wang [36]. From the observation of ion emission it is not possible to determine when the ion is formed during the reation.

In Fig. 10 the two timescales are shown as a function of the distance from the surface. the shaded area corresponds to the time space domain for which freezing is expected in a reactive scattering experiment of the type $X_2 + M \xrightarrow{+e^-} MX + X^-$. It can be seen that the freezing distance is expected to vary between 8 and 12 Å. This variation depends on the electronic properties of the surface and in particularly on the characteristic length scale l_0, the lifetime broadening Δ_0 and on the velocity of the outgoing nucleus. This velocity in turn depends on the history of the scattered nucleus and implicitly on the electronic structure that governs the forces on the nuclei involved. It is important where the incoming molecule is harpooned and how strongly it has been accelerated in the course of the dissociation reaction. The importance of the incoming trajectory was not discussed in a recent paper of Böttcher et al. [80]. However, they correlated the observed O^- yields from the reaction of O_2 with Cs with singlet to triplet conversion rates of metastable He* atoms scattered at the same surface. These conversion rates are known to be very sensitive to the density of states at the surface and the Fermi level and are an excellent probe for the outermost electronic structure of a surface that is experienced by an impinging molecule [81].

A complete model for ion emission includes the velocity distribution of the products. If the potential energy surfaces and the transition points where the system jumps from one to the other were known, it is an easy task to determine the velocities by integration of the equation of motion. For the case of O^- emission in the reaction of O_2 with Cs, Wang [36] constructed two potential energy surfaces and calculated trajectories for the reaction. The implementation of the velocity distribution in a Newns–Anderson formalism [72,82] then allows the calculation of the ion emission probabilities. It was shown experimentally [71] and theoretically [70] that these probabilities follow to first order an $e^{-v^*/v_\perp}$ law. However, deviations are expected from this law as soon as the lifetime broadening (see Fig. 10) levels off [72]. The value of v^* is characteristic for the process and related with l_0 and τ at the freezing distance. For ion scattering it is found to be about $2 \pm 1 \times 10^5$ m/s [69]. For the case of reactive scattering, where the electronic motion at the freezing distance is slow, the v^* values are expected to become smaller.

2.2.3. *Auger de-excitation*

After the observation by Gesell, Arakawa and Callcott of exoelectron emission upon chemisorption of oxygen and water on fresh Mg surfaces, Ehrlich suggested that the emission process is related to the Auger effect, where two electrons annihilate a hole state [21]. Ferrante confirmed exoemission from a clean, annealed Mg(0 0 0 1) single crystal [22] and therefore excluded stress related electron emission. He recalled the Auger de-excitation idea and proposed that the "chemical interpretation" was also the explanation for the chemiluminescence in the $Mg + O_2$ reaction [23]. Starting from the Nørskov, Newns and Lundqvist model [1] formulated for chemiluminescence in the halogen + alkali metal systems, Kasemo et al. [57] outlined a model in which the electron emission process is related to Auger de-excitation of a hole state below the Fermi level that is formed during adsorption (see Fig. 11).

In this picture the hole is bound to a reacting molecule or atom and forms an excitation that may lead to electron emission. Energy conservation thus implies that holes deeper below the Fermi level than the work function are created during the adsorption process.

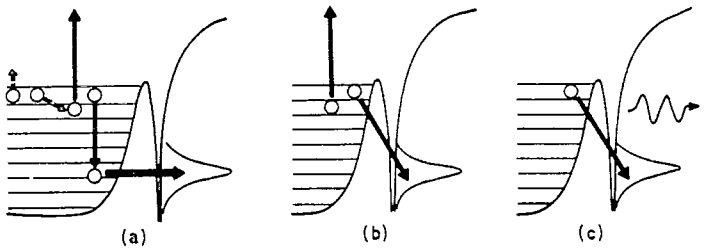

Fig. 11. The Kasemo picture: Schematic illustration of three decay processes of the intermediate hole state resulting in electron (a) and (b) and photon emission (c). From [57].

In contrast to the case of negative ion formation the modeling of the Auger induced electron emission is more complex, since the problem involves several electrons and large excitations. The Auger effect [83] is a radiationless de-excitation channel for an electronic excitation. It involves the scattering of two occupied states $\Psi_{1i}(E_1, k_1)$ and $\Psi_{2i}(E_2, k_2)$ into two unoccupied states $\Psi_{1f}(E_{1'}, k_{1'})$ and $\Psi_{2f}(E_{2'}, k_{2'})$. Energy and momentum are conserved [84]. So it is sufficient to characterize the Auger decay by three of the four involved states since the fourth state is determined. In the nomenclature for Auger decays the first state is the excitation, the second is the initial state of the electron that annihilates the excitation and the third is the initial state of the electron that is emitted into the vacuum. In Fig. 12 the Auger decay is shown in a one electron energy–momentum diagram. The initial states are free electron-like states on a parabola. It is evident that the excitation should not be part of the same band since without "umklapp" processes, i.e. the involvement of the lattice, energy and momentum can only be conserved for exchange reactions in which $\Psi_{1i} = \Psi_{2f}$ and vice versa. Thus, no emission into the vacuum can be observed and any electron emission must involve at least two bands. This condition is met where the excitation is localized on an atom or molecule, as shown in Fig. 12 as a dispersion free band.

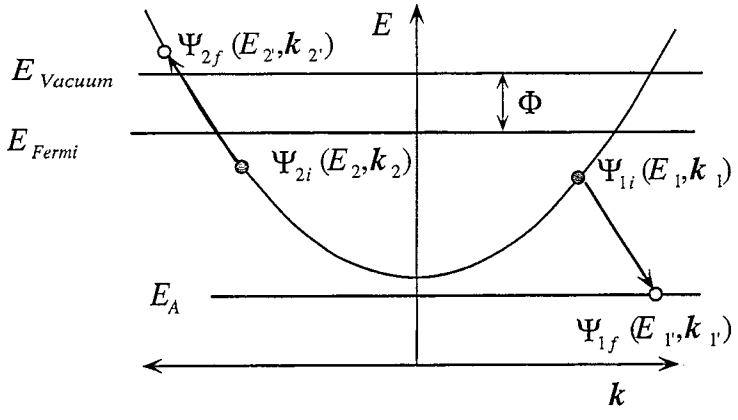

Fig. 12. One electron energy picture for the Auger effect in a simple band structure. Energy and momentum conservation strongly favor an emission in the vacuum if two different bands such as the free electron band and the localized hole state at E_A are involved.

The matrix element for the de-excitation process can be written as

$$M_{\text{Auger}} \propto \left| \left\langle \Psi_{1f}, \Psi_{2f} \left| \frac{e^2}{r_{1,2}} \right| \Psi_{1i}, \Psi_{2i} \right\rangle \right|^2 \delta(E_1 + E_2 - E_{1'} - E_{2'}) \delta(\boldsymbol{k}_1 + \boldsymbol{k}_2 - \boldsymbol{k}_{1'} - \boldsymbol{k}_{2'}), \qquad (5)$$

where the last two terms guarantee energy and momentum conservation and where $e^2/r_{1,2}$ is the operator for the Coulomb interaction. From this the Auger de-excitation spectrum can be calculated. Under the assumption of a constant matrix element and a constant density of states the kinetic energy distribution of the electrons in the solid $S(E_m)$ is for $E_x \geq E_m > -\Phi$ proportional to $(E_x - E_m)/(E_x + \Phi)$, where the measured energy E_m is $E_{2'}$ and E_x corresponds to the excess $E_F - E_{1'} - \Phi$(where all E-values are given relative to the vacuum level).

Prince et al. first extracted the excess energy from the work function information and from the variation of the exoelectron yield [58,59,85]. They developed a static model for the Auger electron yield near threshold and arrived at a cubic power law $Y \propto (\varepsilon_A - \Phi)^3$ [59]. Later, a value of $\frac{5}{2}$ for the exponent was found [33]. The difference is due to the different expansions used to solve the convolution integral between the Auger electron energy distribution inside the solid and the escape function (cf. Section 2.2.1). In the Prince model the excitation, i.e. a hole on the atom or molecule, is injected instantaneously at its final energy ε_A. This is only valid if the electronic lifetimes are long compared to the time in which the nucleus creates the excitation.

In the case of the oxidation of Li a power law $Y \propto (\varepsilon_A - \Phi)^\kappa$ was fitted to the kinetic data (see Fig. 35). Values of $\varepsilon_A = 4.4 \pm 0.5$ eV and $\kappa = 5.8 \pm 1.5$ were found [51]. The ε_A value was in good agreement with cluster calculations in which an electron transfer on an O^- ion in a Li cluster is predicted to release an energy of 4.5 eV [27].

The chemical hole diving model [33] was developed to provide a more quantitative understanding of these findings. The main purpose of this model was to find a link between a microscopic description for the non-adiabatic electron yield and observable dynamic parameters such as the hole injection time and the hole lifetime of the process. Fig. 13 shows a dynamic correlation diagram which depicts the injection process of an affinity level into the Fermi sea.

The probability for exoelectron emission will depend on the power $\Delta E/\Delta t$ for the injection process. This implies that the reaction time Δt can be determined from the emission probability, the value of ΔE and the work function Φ. The emission probability and the work function change can be measured directly from the emitted exoelectrons. The values of ΔE are reflected in photoemission spectra where it is identified with the highest occupied orbital (HOMO) of the adsorbate *after* adsorption. In the case of the reaction of O_2 with alkali metals the dive was attributed to the hole on the O 2p shell of the O^- ions that are created in the course of the O_2 dissociation. In Fig. 14 the O2p binding energies as measured with photoemission [86] are plotted versus the bandwidth of the alkali metals A. As can be seen, these energies are closely related to the heat of formation in the reaction of $\frac{1}{2}O + A \rightarrow \frac{1}{2}(A_2O)$. This indicates that almost all enthalpy is released in the transfer of one electron from the Fermi energy into one atomic oxygen level. In Fig. 14 the work functions of the clean alkali metals are also shown. They also decrease with decreasing Fermi energy and are smaller than the O 2p binding energies. Therefore the necessary condition $\Phi < E_B(O\ 2p)$ (i.e. energy conservation) is met for the emission of exoelectrons via Auger de-excitation.

The model consists of three steps: (i) excitation, (ii) Auger de-excitation and (iii) electron emission into the vacuum. (i) The excitation is a hole that dives by an energy $\varepsilon_x(t)$ into a homogeneous electron

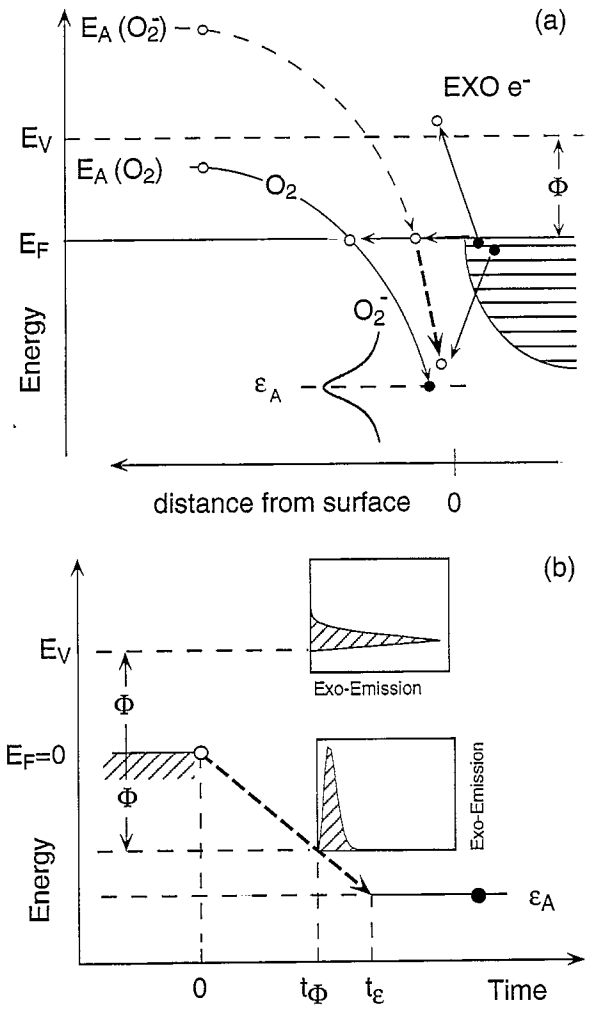

Fig. 13. (a) One electron picture for the injection of an affinity level below the Fermi level for the case of O_2 on alkali metals. As soon as intermediate O_2^{2-} is formed via two resonant electron transfers, the molecule bursts and the holes on the O^- fragments start to dive below the Fermi level. The de-excitation of such a hole may lead to Auger emission of an exoelectron. (b) Model for the chemical hole diving process. The reaction starts at $t = 0$ and ends at $t = t_\varepsilon$, i.e. when the hole state has reached its maximum binding energy ε_A. As soon as the hole survives an injection deeper than the work function ($t > t_\Phi$), exoelectron emission through an Auger de-excitation into the vacuum is possible. The insets show schematically the exoelectron distribution in energy and time, respectively. From [33].

gas. Since the excitation is carried by a chemisorbing species the effect is localized at the surface. The diving is supposed linear in time

$$\varepsilon_x(t) = \frac{\varepsilon_A}{t_\varepsilon} t, \tag{6}$$

where ε_A is the maximum binding energy of the affinity level and t_ε is the time for the injection of the affinity level to ε_A. (ii) The Auger de-excitation starts for $\varepsilon_x > 0$ and is proportional to the available

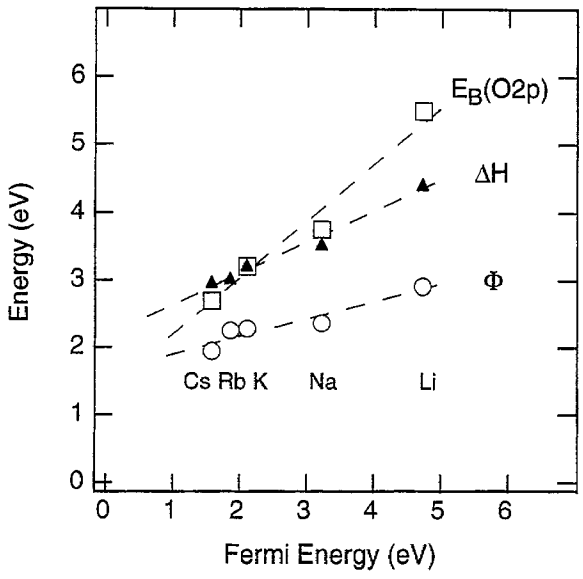

Fig. 14. Plot of the O 2p binding energies, the heat of formation ΔH ($\frac{1}{2}O + A \rightarrow \frac{1}{2}(A_2O)$) of the alkali oxides and the work functions Φ of the clean metals versus the bandwidth (Fermi energy) of the alkali metals.

phase space for de-excitations, i.e. the lifetime τ of the excitation that is proportional to ε_x^{-2}. Steps (i) and (ii) therefore determine the time dependent survival probability P_h of a localized hole in an electron gas. It was found that

$$P_h(t) = e^{-t^3/3t_\varepsilon^2\tau_\varepsilon}, \tag{7}$$

where t_ε is the diving time down to ε_A and τ_ε is the hole lifetime at ε_A. The factor $\frac{1}{3}$ is a consequence of the integration of the decay rate dP_h/dt, which is proportional to the square of the time.

The kinetic energy distribution of the Auger electrons inside the solid $S(\varepsilon)$ is proportional to

$$S(\varepsilon) \propto 1 - \frac{\varepsilon}{\varepsilon_x}, \tag{8}$$

where ε_x is the center of gravity of the hole at time t and where $\varepsilon \leq \varepsilon_x$ and is measured with respect to the Fermi energy. In principle the whole electron–hole pair cascade that is initiated by the de-excitation should be implemented in a complete description of the de-excitation process. Since only the highest excitations may yield to electron emission into vacuum it is a good approximation to neglect all further generations in the cascade. If we take for example an energy ratio ε_x/Φ of 1.1 then we find that after the first cascade step less than 1% of excitations are still larger than the work function. In the emission step (iii) the refraction of electrons at the inner potential of the solid creates a high pass filter for electrons with kinetic energies exceeding the inner potential. The simplest model for this refraction assumes an isotropic Auger electron energy distribution and a step function for the inner potential. It then follows that the emission is proportional to the momentum of the electrons in the vacuum [65] or proportional to the solid angle of the total reflection cone. From

(ii) and (iii) it is straightforward to determine the spectrum of the Auger de-excitation outside the solid. Substituting $\varepsilon = E_m + \Phi$ in Eq. (8) and with yield $Y \propto \sqrt{E_m}$ (cf. Section 2.2.1) we get

$$Y(E_m) \propto \sqrt{E_m}\left(1 - \frac{E_m + \Phi}{\varepsilon_x}\right), \quad 0 \le E_m \le \varepsilon_x - \Phi. \tag{9}$$

where E_m is the measured kinetic energy with respect to the vaccum level, Φ the work function and ε_x is the excitation energy of the hole leading to Auger de-excitation. Integration of Eq. (9) over all energies gives a total yield proportional to $(\varepsilon_x - \Phi)^{5/2}$ (cf. Section 2.2.1). In Fig. 15 the calculated yield is shown as a function of the parameter ε_A/Φ. For a given reaction time $t_\varepsilon/\tau_\varepsilon$ and affinity ε_A the yield decreases with increasing work function.

Furthermore the reaction time t_ε in units of the lifetime τ_ε of the hole at ε_A strongly affects the non-adiabatic electron emission in the expected way, i.e. the non-adiabatic yield increases with decreasing reaction time. The finite lifetime τ_ε causes via the Heisenberg uncertainty principle an energy broadening γ_ε. In Fig. 15 it can be seen that a large broadening $\gamma_\varepsilon/\varepsilon_A$ increases the non-adiabatic yield since the yield increases non-linearly with the excess energy. When the results as shown in Fig. 15 are compared with the experimentally observed exoelectron emission probabilities they yield a normalized reaction time $t_\varepsilon/\tau_\varepsilon$ (cf. Section 4.2).

The lifetime broadening of the injected affinity level has been implemented into the chemical hole diving model. It turns out that this broadening only weakly affects the exoelectron yield (see Fig. 15). It is, however, important for the energy spectra of the exoelectrons. The lifetime broadening γ_ε affects the energy distribution of the emitted electrons and, in principle, the hole lifetime τ_ε may be determined from the kinetic energy distribution of the exoelectrons. This enables one to determine the frequency of the internal clock τ_ε^{-1} and to derive an absolute timescale for the reaction. It is problematic to determine a lifetime from an energy broadening. In this case all extra broadening that, for example, arises from thermal effects are excluded, since the process is so fast that it does not couple to the heat bath of the solid. From the argument mentioned above it becomes clear that

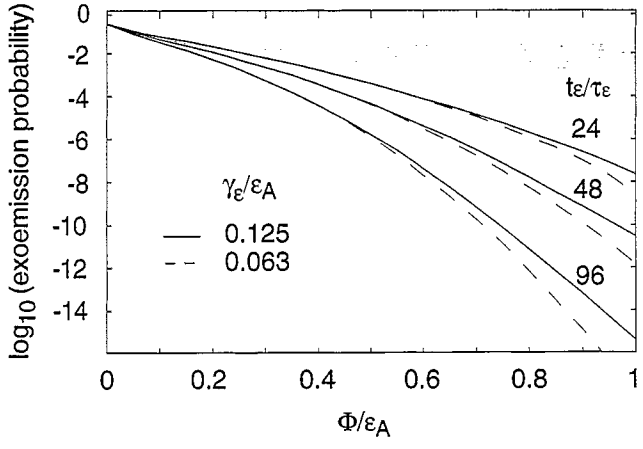

Fig. 15. Calculated exoelectron emission probabilities versus the ratio between the work function Φ and the maximum binding energy of the affinity level at ε_A. The lines represent curves for different reaction times in units of the hole lifetime at ε_A. The difference between the solid and the dashed lines is the different energy broadening. From [33].

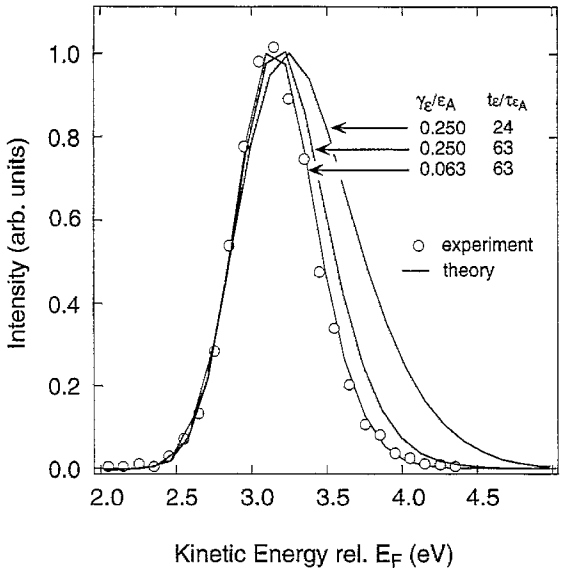

Fig. 16. Electron energy distributions for exoelectrons in the Li + O_2 reaction. The experimentally observed width reflects in the theory of Ref. [33] a hole lifetime.

secondary de-excitations from the electron–hole pair cascade should not contribute to the exoelectron emission. It is mainly governed by primary de-excitations and therefore the energy spectra should be very narrow and pinned at the vacuum level. In Fig. 16 such theoretical energy spectra are shown and compared with experiment.

In a recent paper Hellberg et al. [37] proposed a theory for Auger electron emission during the reaction of Cl_2 with K. They also used a trajectory of an affinity level below the Fermi level for the description of the de-excitation. The lifetime was described with an exponential Auger rate $\tau_{\mathrm{Aug}}^{-1} = A_0 \exp(-\alpha_{\mathrm{Aug}} z)$ where A_0 and α_{Aug} are constants and z is the distance from the surface [87]. The energy distribution curves were obtained by projecting the $Cl \rightarrow Cl^-$ rate onto the energy axis. By doing this they were able to explain experimental data that indicated a shift of electron emission curves as a function of the Cl_2 kinetic energy. It must be noted that the authors' assumptions as to the distribution of Auger electron energies of Ref. [37] are too simple. The Auger spectrum from the de-excitation of a localized hole in an electron gas is not expected to be a function that peaks at the excitation energy, as is for example the case in photoemission from a localized state. The Auger de-excitation spectrum merely corresponds to the first cascade step of the de-excitation, which is a spectral function like that in Eq. (9).

2.3. Comparison between Auger and photo de-excitation

The Auger effect can be understood in terms of classical collisions [84]. Two occupied states with energy E_i and momentum $\hbar \boldsymbol{k}_i$ are represented by $(E_1, \boldsymbol{k}_1)$ and $(E_2, \boldsymbol{k}_2)$, and scatter into two unoccupied states $(E_{1'}, \boldsymbol{k}_{1'})$ and $(E_{2'}, \boldsymbol{k}_{2'})$, respectively. In the process energy and momentum are

conserved, i.e. $(E_1 + E_2, \boldsymbol{k}_1 + \boldsymbol{k}_2) = (E_{1'} + E_{2'}, \boldsymbol{k}_{1'} + \boldsymbol{k}_{2'})$. For electrons and other Fermions the final states have to be empty before the scattering event.

Chemiluminescence and the photoeffect have no classical analogy since in the process particles (photons) are generated or annihilated. In the photo de-excitation only one initial and final electron states $(E_1, \boldsymbol{k}_1)$ and $(E_{1'}, \boldsymbol{k}_{1'})$ are involved. Energy and momentum conservation implies $(E_1, \boldsymbol{k}_1) = (E_{1'} + \hbar\omega, \boldsymbol{k}_{1'} + \boldsymbol{G})$ where $\boldsymbol{G}$ is a reciprocal lattice vector. In Fig. 18 $\boldsymbol{G} = 0$ is shown. Note that in principle, a reciprocal lattice vector could also be involved in the case of the Auger transition.

In Fig. 17 the Auger collision is compared with the photon emission (chemiluminescence) that is encountered in the case of the de-excitation of a localized hole state by an electron gas. The free electron dispersion follows $E = (\hbar\boldsymbol{k})^2/2m$, while the localized hole state has no dispersion, i.e. $E_A = \text{const}$. For both de-excitations two different bands i.e. free electrons and localized states are essential. In a single band situation photon emission is not allowed, at least as long as all valence electrons sit in the first Brillouin zone. Without the involvement of a reciprocal lattice vector the Auger transitions would not yield enough momentum transfer to the electron that must escape the solid. The two transition modes are different. In chemiluminescence all transitions are vertical since the photon momentum is neglected, while for the Auger de-excitation electron momentum has to be transferred to the electron that is emitted.

Another important difference between light and Auger electron emission is the rate at which the processes occur. The branching ratio, i.e. the ratio of chemiluminescence and Auger recombination rates, is very useful for the identification of the particular process leading to non-adiabatic particle emission.

The ratio of the radiative and Auger recombination rates Γ_{rad} and Γ_{Auger} is

$$\frac{\Gamma_{\text{rad}}}{\Gamma_{\text{Auger}}} \propto \frac{\alpha_0^3}{n a_0^3} \left(\frac{\varepsilon_x}{E_{\text{Rydberg}}} \right)^{\kappa}. \tag{10}$$

The $n a_0^3$ term is the electron density in atomic units, α_0 the fine structure constant and $(\varepsilon_x/E_{\text{Rydberg}})^{\kappa}$ is the excitation energy dependence. The dependence on the density is clear from the above. The Auger rates involve the product of the densities of initial states $(E_1, \boldsymbol{k}_1)$ and $(E_2, \boldsymbol{k}_2)$ since two electrons have to collide in order to eject an Auger electron. On the other hand the chemiluminescence rate is proportional to the density of initial states $(E_1, \boldsymbol{k}_1)$ that fill the hole. The density of final states cancels

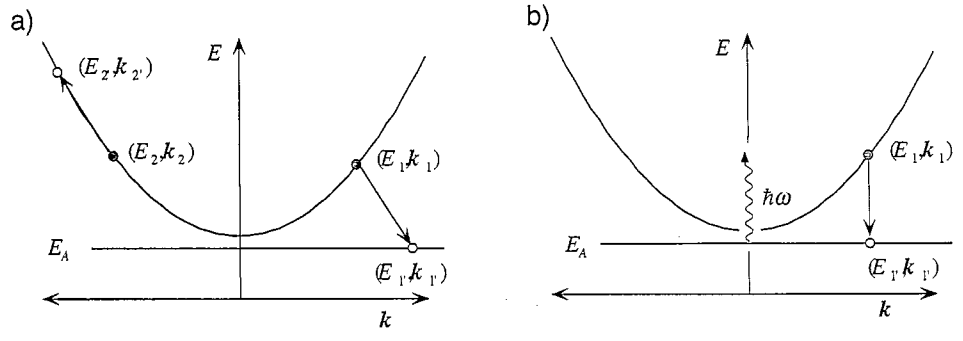

Fig. 17. One electron energy picture of (a) the Auger effect and (b) the chemiluminescence in a simple band structure.

for the comparison of the rates. The hole density $(E_{1'}, k_{1'})$ that describes the excitation is the same for both processes and the final state density of the Auger electron $(E_{2'}, k_{2'})$ is implicitly given by the initial state density. This density dependence is particularly interesting at surfaces where the electron densities increase from zero to the bulk value and it is therefore expected that the branching ratio should depend strongly on the distance from the surface.

The optical transition rates are suppressed by the much smaller density in the photon phase space compared to that of the electrons, by a factor of third order in the fine structure constant $\alpha_0 = e^2/\hbar c = 1/137$.

Finally the energy dependence is discussed. The exponent κ is larger than unity since the wavelength of the photons decreases faster with energy than that of the electrons. It does, however, vary from case to case. For the de-excitation of core holes, for example, an exponent $\kappa = 2$ is found [88] if the Auger rate is independent of energy. Landsberg and Adams derived an exponent $\kappa = \frac{7}{2}$ for the recombination of a conduction band electron with a hole acceptor, where they found an ε_x^2 dependence for the radiative recombination rate and an $\varepsilon_x^{3/2}$ dependence for the Auger rate [89].

For spontaneous photon emission and a constant matrix element the chemiluminescence is proportional to ω^3 [1,50]. It is, however, not possible to give an exponent for Auger electron emission into the vacuum since the work function implies a threshold for the Auger emission rate [33]. Therefore no exponent κ can be given for this case.

3. Kinetics

Non-adiabatic particle emission is a response of a system to an external perturbation. This response is a measure of the reaction rate that proceeds along non-adiabatic branches. From the observation of the emission rates kinetic models can be developed and intermediate products may be identified. One particular advantage of using non-adiabatic particle emission as an experimental tool for the investigation of reaction parthways is that the reaction is not perturbed by its observation since non-adiabatic particles are produced intrinsically in the reaction. On the other hand the interpretation of non-adiabatic particle emission rates as reaction rates is complicated by the fact that the emission probability is not constant and that the emission does not necessarily stem from the same process. For example, in the case of charged particles the work function strongly influences the emission rates. The work function can, however, be determined directly from the energy distribution of the non-adiabatic particles and thus yields additional information.

The external perturbation of the system stimulates the reaction under investigation. These stimulations range from friction, light and gas pulses to temperature variations. In this section the two latter cases are discussed.

Fig. 18 shows the exoelectron response of one monolayer of Cs on Ru(0 0 0 1). Shown as a function of time are (a) the exoelectron yield, (b) the sample temperature indicating thermal stimulation and (c) the chemical stimulation, i.e. exposure of O_2 from the gas phase. The emission of particles upon heating the sample with no oxygen in the gas phase clearly indicates the existence of a metastable surface species that decays under the emission of electrons (cf. Section 3.2.1).

Since kinetics are macroscopic manifestations of a reaction they do not allow an unambiguous identification of the microscopic reaction mechanism. Therefore the discussion of microscopic models for non-adiabatic particle emission is postponed until Section 4.

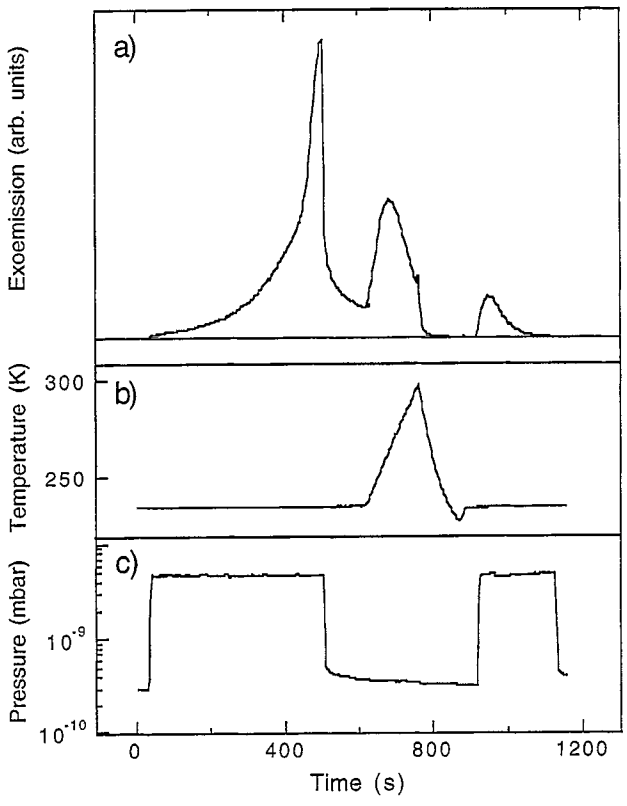

Fig. 18. Emission of exoelectrons from 1 ML of Cs on Ru(0 0 0 1) as a function of time (a) under varying temperature (b) and O_2 partial pressure programs (c). From [115].

3.1. *Chemically stimulated particle emission*

Chemically stimulated particle emission was first observed by Thomson [7]. There was a long debate as to whether the adsorption process triggers the non-adiabatic particle emission from metastable structures such as defects or precursor states that were already present on the surface or whether the adsorption process itself leads to particle emission. The existence of the first possibility is confirmed, for example, by OSEE where electron emission can be observed with photons of an energy lower than the work function of the surface [61,90]. The latter hypothesis, i.e. the emission of particles from the gas surface reaction with a substrate in its lowest energy state, is much more difficult to verify and only became accepted upon the use of single crystals and ultra high vacuum (UHV) technology. It must be mentioned that the requirement of a clean substrate without metastable structures can only be met in the very first reaction stage. Therefore it is important to study the onset of non-adiabatic particle emission. If the non-adiabatic particle emission starts from the very beginning of the reaction it is a candidate reaction without precursor state. As will be seen in the following, such reactions take place in the oxidation of alkali metals.

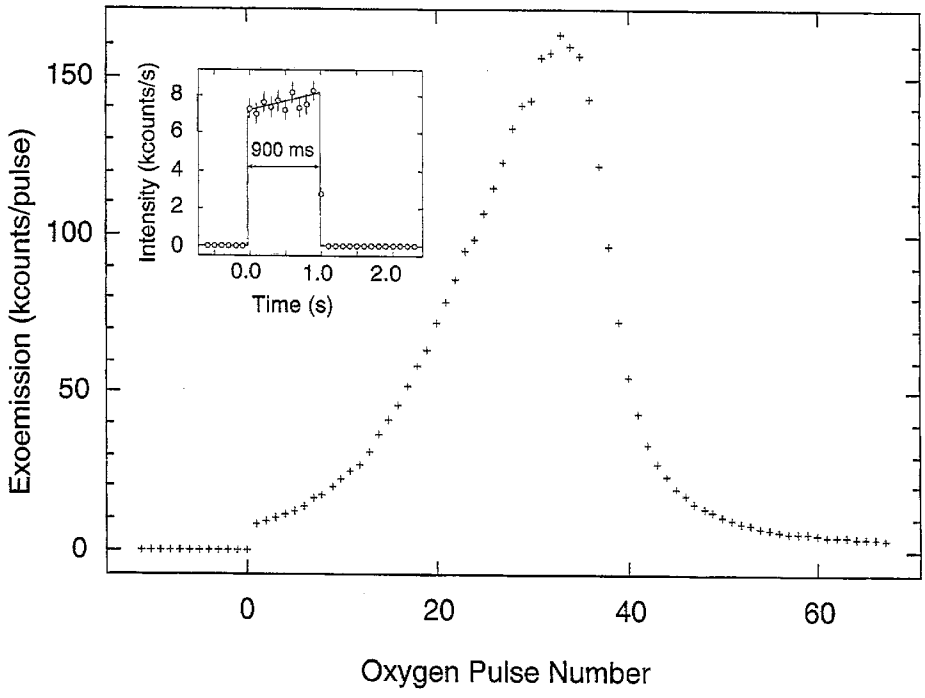

Fig. 19. Exoelectron response from the reaction of a sharp oxygen pulse with Li. The inset shows the response on the first oxygen pulse with a duration of 900 ms.

Fig. 19 shows the negative non-adiabatic particle emission at the start of the oxidation of two monolayers (ML) of clean Li on Ru (0 0 0 1). One pulse of oxygen corresponds to roughly 5×10^{-2} ML of oxygen. The inset shows the non-adiabatic particle current. It has a sharp profile that follows the gas exposure of the chopped molecular beam. This, together with the fact that the initial exoelectron emission rates do not appreciably depend on the surface temperature has made the $Li + O_2$ system a prototype reaction for the study of direct dissociation [51].

3.1.1. $Mg + O_2$

The reaction of oxygen with both magnesium and magnesium oxide leads to light as well as to exoelectron emission. In a vacuum of 1.5×10^{-3} Pa Lohff and Raether [91] found that negative particles were emitted after abrasion of Mg (and other metals) with a steel brush and that the emission died off after a few hours. This emission was attributed to the formation of oxide on the fresh magnesium surface. In a following paper Lohff showed in experiments with controlled oxygen exposures that the oxygen played a crucial role in the emission [92]. The kinetics of the emission currents I followed a $I \propto t^{-\kappa}$ law where the exponent κ was close to 1 for Mg. Later, Kasemo [23] found the oxidation of Mg to be accompanied by light emission as well. Chemiluminescence for the exposure of MgO surfaces to oxygen has been observed by Roginskii [93]. The emission kinetics were correlated with thermally stimulated oxygen desorption from MgO [41]. The light spectra as found by Coon [40] for the reaction of O_2 with MgO correspond remarkably well with those found

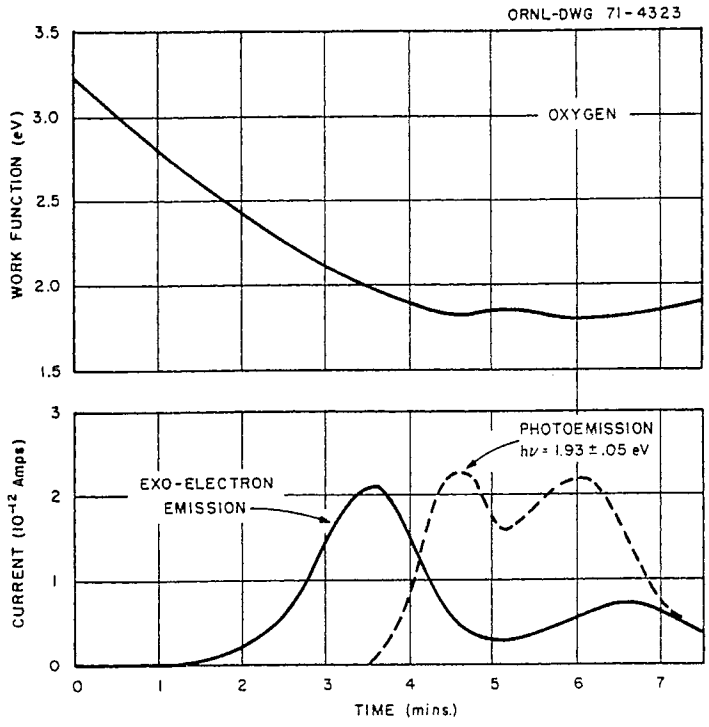

Fig. 20. Time development of the work function, the exoelectron emission, and the photoemission ($h\nu = 1.93 \pm 0.05$ eV) from a fresh magnesium surface. From [99].

for the late stage of oxidation of Mg [23]. Exoelectron emission from O_2 + MgO was observed by Ivankin [94] who found an emission rate proportional to the chemisorption rate of oxygen.

The "metal" community [21,57] and the "oxide" community [39–41,95] differed, however, in their interpretations of the origin of the emission. The "metal" community favored a picture where the electrons and light are emitted by the de-excitation of a hole created below the Fermi level during the reaction [57]. The "oxide" community on the other hand favored a process in which F-centers (i.e. oxygen defects) supply the excess energy for the photon [96] and/or electron emission process [40]. In the case of MgO + O_2, electronic transitions occur at the surface [97] or even in the gas phase above the surface [98]. These different explanations for the emission process do not necessarily contradict each other since different processes may lead to exoemission and/or chemiluminescence. In the case of the oxidation of Cs more than one emission mechanism is at work for electron emission [28,30]. In the following the results of the exposure of clean magnesium to oxygen are reviewed [21,22,57,90,99].

The O_2 + Mg reaction proceeds under emission of electrons [21,99] as well as under emission of visible light [23]. In Fig. 20, the emission of exoelectrons (solid line) is compared to that of photoelectrons (dashed line) as a function of oxygen exposure of the surface [99]. The photoelectrons were excited by 1.93 eV photons. Exoemission currents of about 10^{-6} electrons per O_2 molecule were reported [21]. The yield of the photoemission and the exoemission are related. It also

indicates that the exoemission is strongly modulated by the work function of the surface. The non-adiabatic particle emission peaks close to the work function minimum that is reached after about 1.5 L [22,99,100].

In the range between 7×10^{-6} and 2×10^{-7} Pa partial pressure of O_2 the exoemission peaks at the same exposure of about 1.5 L O_2 [21]. Later Ferrante [22] found that the rate of electron emission is proportional to the oxygen arrival rate. The double peak structure in the emission that was observed by Ferrante was, however, attributed to residual water contaminations and/or to the variation of the electron escape probability due to work function variations. The first exoemission maximum is close to the monolayer formation time as calculated by assuming unit sticking probability [99]. All these observations corroborate a picture in which the formation of the first layer of oxide on Mg is accompanied by the emission of electrons. The observations did not, however, allow a detailed kinetic analysis of the reaction. The variation of the work function during the adsorption and the strong dependence of the exoelectron yield as a function of the local work function do not allow a one to one correspondence between reaction rate and emission yield to be drawn. In energy resolved electron emission spectra Allen et al. [90] discovered the existence of low work function patches. In addition they reported photo excitation of electrons that were trapped above the Fermi level. Grunberg and Wright [61] associated such OSEE with negative ion vacancies (F′-centers).

Kasemo and Törnqvist [100] were the first to study the emission of light (chemiluminescence) and exoelectron emission in the same experimental set up. In Fig. 21 the correlation between the emitted light and the intensity of the simultaneously emitted electrons is shown. After an initial rapid intensity decrease a maximum occurs for both curves close to the work function minimum. The

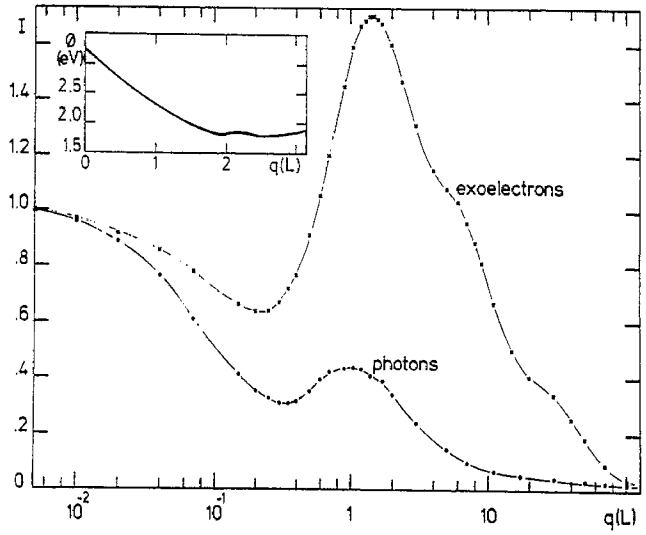

Fig. 21. Normalized light emission and electron emission intensities during O_2 exposure of a magnesium film as a function of gas exposure. The inset shows the variation in work function Φ with O_2 exposure from Fig. 20. From [100].

electron emission maximum appears, however, at a slightly higher oxygen exposure. If the simultaneous presence of electron and light emission processes reflects the presence of alternate de-excitation channels from the same chemical excitation, the differences may be explained in terms of a variation of the work function that affects the electron emission probability in a direct way. In the $Al + O_2$ and $Ti + O_2$ systems [101,102] it was found that at low exposures the light emission rate decays much faster than the rate that is expected when it is assumed that the light emission probability is constant, that every surface site is exoactive and given a constant sticking coefficient. It was attributed to oxygen chemisorption on "active sites" covering a small portion of the surface. This shows how carefully kinetics have to be interpreted and how sensitive they may be for the study of oxidation processes.

In summary it was shown that the kinetics of non-adiabatic particle emission is very susceptible to the status changes of a system, such as $Mg/MgO + O_2$. As with other spectroscopic methods, the single steps have to be identified in order to better understand the oxidation mechanism.

3.1.2. $Cs + O_2$

The oxidation of alkali metals is known to be followed by electron emission [103–105]. This electron emission does not simply follow the emission of photoelectrons reflecting the photoelectric yield dependence on the work function. It therefore comprises additional information about the kinetics of the oxidation process.

Recently Böttcher et al. began to investigate non-adiabatic particle emission from the oxidation of alkali metals. They started with Cs since it is the alkali metal with the lowest work function and is therefore the best candidate for a large yield of negative particles. From the literature it is known that the non-adiabatic particles mainly consist of electrons and not of negative ions [9,103]. It turns out, however, that there is a small probability ($\leq 10^{-8} O^-/O_2$) for ion emission at the beginning of the oxidation of Cs metal [26]. In contrast to the oxidation of Mg the reaction of oxygen with alkali metals proceeds without the emission of light [51]. This conflicts with one reported result in which the reaction of O_2 with Na is claimed to be accompanied by the emission of light [57].

Böttcher et al. [105] measured the non-adiabatic particle yield from a thin Cs film as a function of exposure to oxygen (see Fig. 22). The work function of the surface was measured separately and it was found that the maximum of the exoelectron emission occurred after the minimum of the work function. This minimum is related to the completion of the Cs_2O_2 peroxide phase [106]. The data suggested that in precisely this stage the process of $Cs_2O_2 \xrightarrow{O_2} CsO_2$ formation gives rise to noticeable exoelectron emission. From comparison with metastable He* ($1s^1\ 2s^1$) de-excitation spectroscopy (MDS) data the non-adiabatic particle emission is seen to be related not only with the work function but also and in a more involved way with the electronic structure of occupied and unoccupied states of the outermost surface layer. Since the de-excitation of metastable He* atoms is governed by the same electronic situation as encountered by adsorbing oxygen molecules, the correlation of MDS with non-adiabatic particle emission is particularly useful for understanding the process. For low work function metallic surfaces ($\Phi < 2.7$ eV) the metastable He* de-excitation process mainly proceeds via the resonance between the He 2s states and the substrate states at the Fermi level. The spectral weight of this de-excitation channel is therefore a measure of the degree of metallization of the interface to the vacuum [81,106–108].

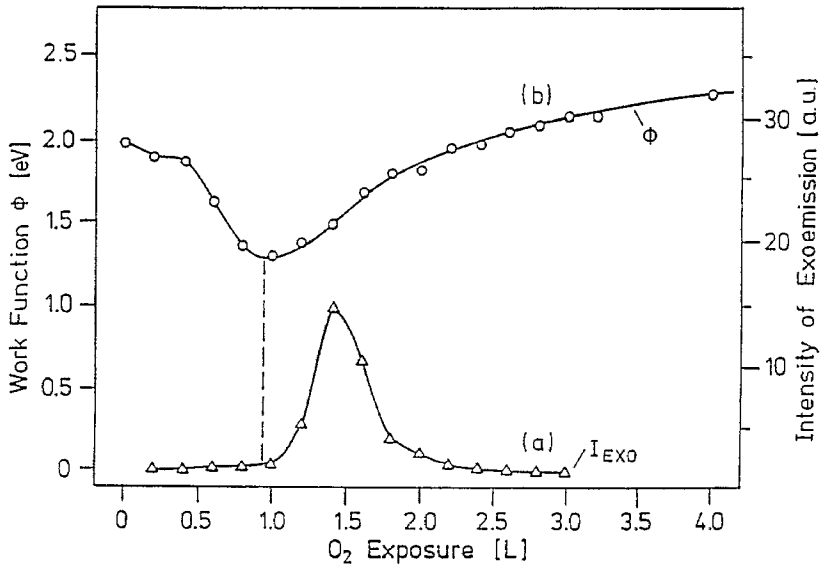

Fig. 22. Variation of the current of exoelectrons (a) and the work function Φ curve (b) upon stepwise exposure of a Cs film with about 3 ML thickness at 220 K to an O_2 pressure of 4×10^{-9} mbar. From [105].

Fig. 23 shows that the non-adiabatic particle emission occurs in parallel with the disappearance of the metallicity of the interface to the vacuum as observed with MDS. This led to the conclusion that efficient non-adiabatic particle emission may only occur on non-metallic but not completely oxidized surfaces where the resonance ionization of $O_2 \rightarrow O_2^-$ is delayed and where enough enthalpy remains for the excitation of an electron above the vacuum level. A kinetic model has been developed that accounts for all observed non-adiabatic particle emission features [109]. All temperature and gas pressure dependencies can be explained within the model, which assumes that the direct impact of an O_2 molecule from the gas phase with an active $Cs_2O_2^*$ complex is responsible for the exoelectron emission.

The exoemission process can be thermally activated for the oxidation of thick bulk films and for one monolayer of Cs on Ru(0 0 0 1) [28]. A metastable O_2^- species on top of the surface was identified as the intermediate species before the exoelectron emission [110] (cf. Section 3.2.1). These findings favored an interpretation of the non-adiabatic particle emission in which a large portion of the oxygen molecules pass an O_2^- precursor before the reaction leads to electron emission.

The electron emission followed by oxygen pulses on one monolayer of Cs on Ru(0 0 0 1) also indicated that a large number of the reacting molecules pass through a long-lived (> 100 ms) metastable state before their decay [111]. Fig. 24 shows the exoelectron current as a function of the number of the oxygen pulse from one monolayer of Cs on Ru (0 0 0 1). The solid dots correspond to emission where the oxygen flux is off. It indicates that a large portion of the exoelectrons stems from long-lived ($\tau > 100$ ms) surface species. The inset shows the response of all oxygen pulses. The non-adiabatic particle response to stimulation by a strong oxygen pulse shows unusual kinetics, since the emission rate decays non-exponentially. An exponential response tail is expected for

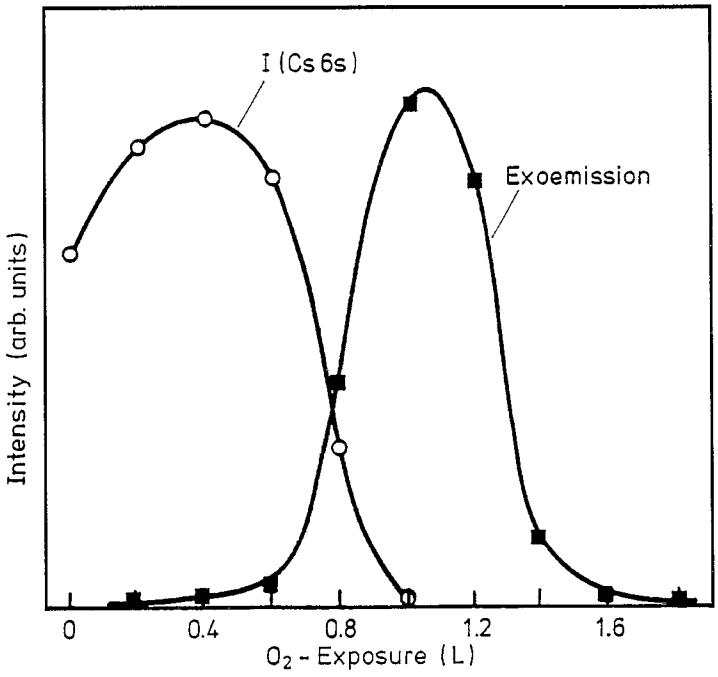

Fig. 23. Variation of MDS intensity from the Cs 6s emission and of the exoelectron current with O_2 exposure. From [105].

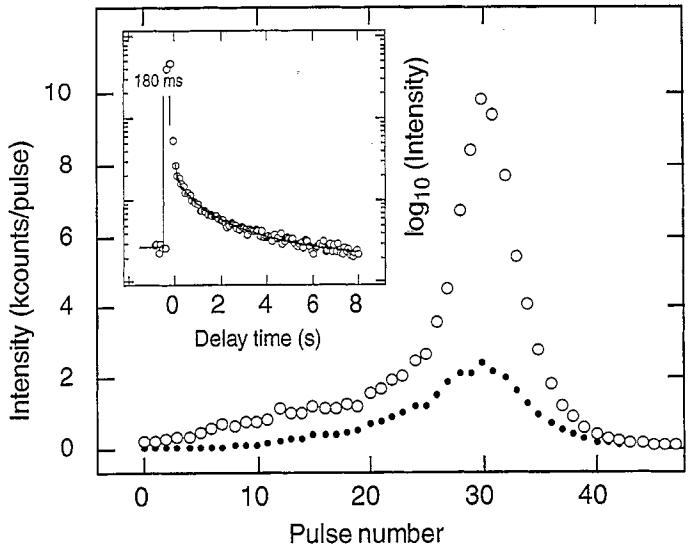

Fig. 24. Exoelectron emission during the oxidation of one monolayer of Cs on Ru(0 0 0 1) at 240 K. The current is given as a function of the oxygen pulse number. One pulse of 180 ms duration consists of 2×10^{13} O_2/cm^2. The inset shows the response of all pulses on a logarithmic scale. The open symbols reflect the total intensity while the solid dots stand for the emission when the gas pulse is off. Data from [111].

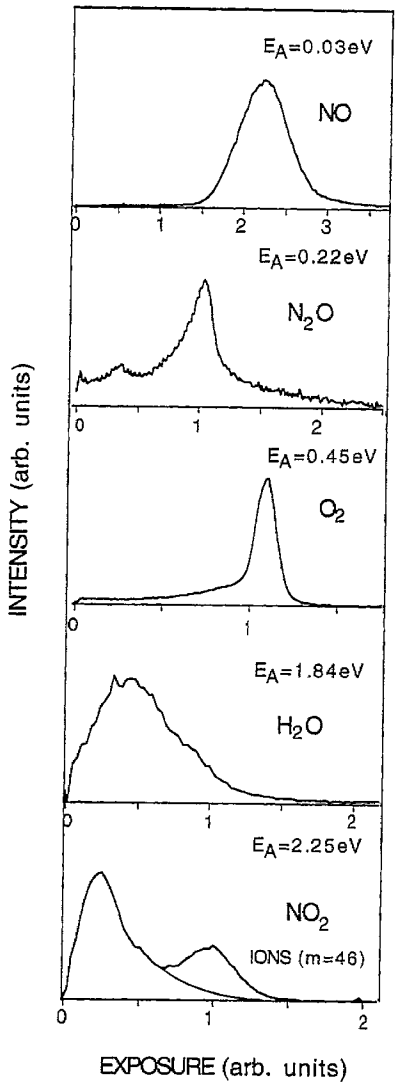

Fig. 25. Negative particle emission kinetics from the reaction of gases with different electron affinities with one monolayer of Cs on Ru(0 0 0 1). The exposure is normalized with the exposure up to the work function minimum that is observed in all five reactions. It is clear that for higher electron affinities the emission occurs at an earlier stage of the oxidation. Note that most negative particles were electrons, where in the case of O_2 and NO_2 negative ions were detected as well [112].

kinetics where the rate is proportional to the number of intermediates (in this case adsorbed O_2^-) and where the number of exoactive sites is constant or much larger than that of the intermediates. From such linear responses it cannot be decided whether the process leading to exoemission is related to diffusion in quasi-equilibrium or to another thermally activated process. If, however, the emission rate is not proportional to the number of intermediates, a first order thermally activated process can be ruled out. Fick's second law implies that the arrival rate at a certain site is not constant if the

spatial distribution of the intermediates changes with time. A non-linear exoelectron emission response to strong oxygen pulses would result from a scenario in which the initial distribution of intermediates given by the adsorption and the spatial distribution of the exoactive sites are not the same. Therefore the non-linearity in the response (see Fig. 24) was taken to indicate surface diffusion, i.e. the restoration of a quasi-equilibrium distribution of the intermediates [111].

The affinity of the impinging molecule plays a crucial role in the kinetics of the emission process. In Fig. 25 the non-adiabatic particle kinetics of different gases from one monolayer of Cs on Ru(0 0 0 1) are shown [112]. The exposures to different gases are normalized with the exposure up to the work function minimum that is commonly observed for all these oxidation processes. It clearly indicates the influence of the affinity on the kinetics of non-adiabatic particle emission. As shown in Fig. 25 the center of gravity of the emission shifts towards higher exposures with decreasing affinity of the reacting molecules. On this qualitative level it is not important to distinguish between the adiabatic affinity and the vertical affinity as outlined in Fig. 3. The non-adiabatic particle emission in the case of NO_2 is particularly interesting since the non-adiabatic particles that are emitted at the work function minimum are NO_2^- ions [75]. This suggests that in the oxidation process of Cs with NO_2, NO_2 may dissociate under the emission of an exoelectron on metallic Cs up to the work function minimum. The reaction with a partially oxidized surface leads to a sharp peak of negative ions that was discussed in more detail in Section 2.2.2. For the case of the reaction of O_2 with Cs, O^- emission was also observed [26,30,80]. The kinetics of the O^- emission follows a first-order kinetic law in which the rate is proportional to the number of unreacted metallic sites. This can be seen in Fig. 26 where the initial O^- emission rate decay is proportional to $\exp(-d/d_0)$ where $d = \int p\,dt$ is the oxygen exposure with $d_0 = 0.7$ L. Assuming unit sticking probability this value indicates that an O_2 molecule inhibits 3.6 ± 1 Cs atoms. The little buckle at the work function minimum is not explained with these kinetics. Similar first-order kinetics were reported by deBlasi et al. [56] for the emission of halogen ions from reactions with metallic surfaces. The case of O^- emission was further investigated for submonolayer quantities of Cs on Ru(0 0 0 1) by Böttcher et al. [80]. They showed that the

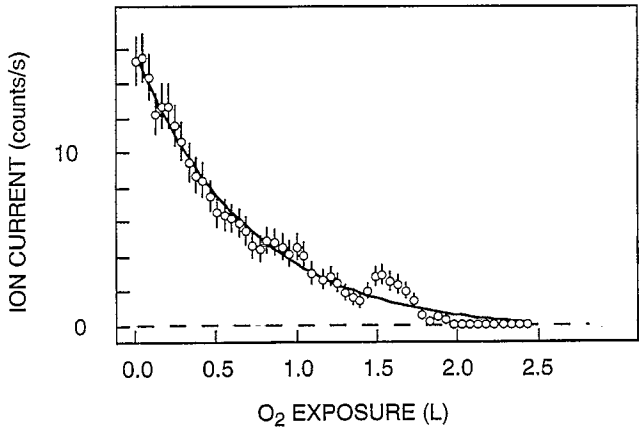

Fig. 26. O^- emission from a monolayer of Cs on Ru(0 0 0 1) as a function O_2 exposure. The applied O_2 pressure was 10^{-6} Pa and the sample was kept at 200 K. From [26].

kinetics do not follow a simple exponential dependence. This is another indication that the formation of surface structures may influence the yield of negative ions. Whether this is related to the formation of an intermediate state or whether the reacted oxygen affects the yield cannot be decided from these kinetics.

3.2. *Thermally stimulated particle emission*

The annealing of an oxidized surface may yield electron emission [113] kinetics similar to those of the "glow curves" that are observed in thermoluminescence [25]. This is a clear indication that such structures are not in thermal equilibrium since thermal stimulation may lead to relaxation under the emission of energy quanta that are large compared to $k_B T$.

Form an analysis of the emission kinetics the activation energies and the kinetic order of the process can be derived. The kinetic simulations are simplified by the fact that the back reaction in the step that leads to exoemission may be neglected, since the released energy exceeds the work function and is therefore much larger than $k_B T$. A detailed identification of the process must, however, involve spectroscopic techniques. To date the Cs + O_2 system is the most extensively studied surface system and is reviewed in Section 3.2.1 [28,105,109,114,115]. The NO + Cs system that shows as well a pronounced temperature dependence on the exoelectron emission yield is not discussed [75].

3.2.1. *The Cs + O_2 system*

The oxidation of Cs is accompanied by the emission of exoelectrons [103]. Studies of the oxidation of thick (i.e. bulk) Cs films revealed that electron emission is essentially confined to the last oxidation step, namely the transformation of peroxides A_2O_2 into superoxides AO_2 [105,109]. A pronounced influence of the sample temperature suggests that thermally activated surface processes are involved. Subsequent experiments with the oxidation of Na films [116] showed a similar behavior while the oxidation of thin Li layers has different kinetics. This is consistent with the fact that Li does not form a superoxide [51]. In contrast to Cs and Na the exoelectron emission from Li did not show a pronounced surface temperature dependence and indicated a second non-adiabatic reaction channel in the first oxidation step, i.e. the formation of A_2O-like compounds. Fig. 27 shows the comparison between the exoelectron emissions from Cs and Li, respectively. The total emitted charge from Cs is larger and the emission peaks at about twice the exposure of Li. The inset in Fig. 27 shows that the emission, although faint, starts in the first oxidation stage where that from Li exceeds that from Cs. Additionally it was demonstrated that the emission of electrons was not restricted to thick layers but also occurs for submonolayer quantities of alkali metals heavier that Li on transition metal surfaces [28,114,116]. However, the probability for the emission of an exoelectron drops by several orders of magnitude in going from thick films to monolayer and submonolayer systems.

A well-defined system is given by a Cs monolayer chemisorbed onto a Ru(0 0 0 1) surface [117]. In this prototype system the nature of the emission step in the last oxidation step could be identified [28]. Extensive low energy electron diffraction (LEED) [118], high resolution electron energy loss spectroscopy (HREELS) [110] and scanning tunneling microscopy (STM) [119] studies of the oxidation of Cs mono and submonolayer systems suggest that the oxidation of Cs on Ru is a complex process invoking the formation of a number of different oxide structures. In the following,

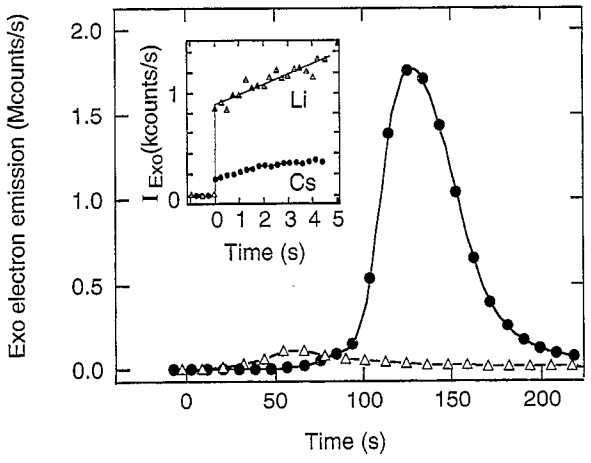

Fig. 27. Experimentally observed exoemission curves for the oxidation of thick layers of Li and Cs. The inset shows that emission starts in the first oxidation stage where the O_2 molecules meet an electron gas.

experiments that start from a well-defined monolayer of Cs on Ru(0001) are discussed [115]. Exoemission is not necessarily an instantaneous process linked to the impact of a particle from the gas phase, but may involve metastable surface species which act as "precursors" and undergo thermally activated transformation. The participation of a surface intermediate with finite relaxation time becomes evident from the results of an experiment displayed in Fig. 18. At $t = 0$ the O_2 partial pressure (panel c) is switched to a value of 5×10^{-7} Pa while the temperature (panel b) is kept at 220 K. The yield of exoelectrons (panel a) rises continuously up to a maximum at the work function minimum where the supply of O_2 from the gas phase is switched off. The exoelectron current does not drop immediately to zero (as would be expected if electronic de-excitation were to take place during the collision with the surface of the impinging O_2 molecule), but continues for quite some time. Moreover, a subsequent linear rise of the temperature up to 300 K causes another burst of exoelectrons. This effect is definitely not due to thermionic electron emission, since the emission current shows a maximum (at 260 K) instead of continuously rising with temperature, while the work function changes by no more than 0.05 eV. The treatment shown in Fig. 18 does not exhaust the capacity for exoelectron emission, as becomes evident from further yield upon readmission of O_2 after the initial temperature has again been reached.

A series of experiments has shown a shift of the temperature for maximum emission, T_m, with increasing heating rate β. In analogy with the analysis of the thermal desorption spectroscopy (TDS) data, a plot of $\ln(T_m^2/\beta)$ versus $1/T_m$ yields a straight line from the slope of which an activation energy of $E^* = 0.8 \pm 0.1$ eV can be derived. Under the assumption of a quasi-first-order process a frequency factor $\nu = 10^{13\pm1}$ Hz was derived from the same data [115]. This is the usual order of magnitude for such processes.

In order to elucidate the nature of the precursor species, spectroscopic methods were applied to the problem. In a HREELS study Shi et al. [110] observed an O_2^- molecular ion on a cold preoxidized Cs monolayer on Ru (0001). As shown in Fig. 28 this species disappears upon

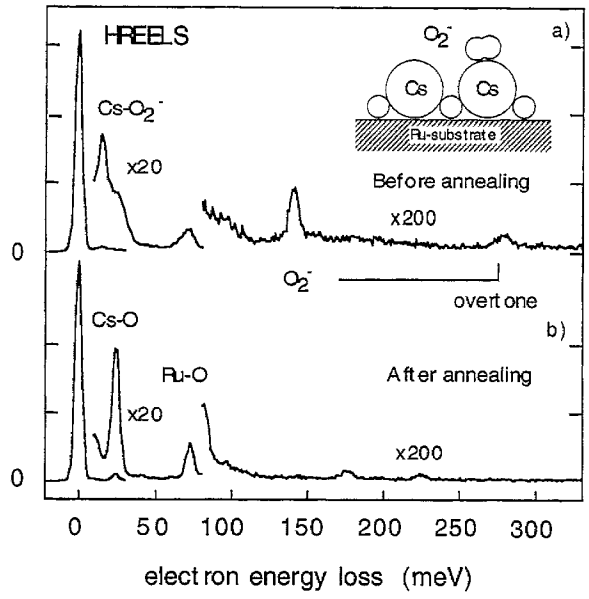

Fig. 28. HREELS spectra of an oxygen treated monolayer of Cs on Ru(0001). The $Cs-O_2^-$(15 meV) and the O_2^-(140 meV) related loss features in (a) disappear on annealing the sample (b). From [28].

annealing to room temperature. From the anharmonicity of the potential, as reflected by the energies of the overtones, the dissociation energy D of the O_2^- species was derived. Taking a Morse potential, the dissociation energy D of the O_2^- molecule is 3.9 ± 0.3 eV, a value close to that of the free ion (4.1 eV). This is an indication that the O_2^- species, also called Jacobi particles [120], are "ionisorbed" on top of the surface, i.e. are bound via the image potential electrostatically to the surface.

By means of X-ray photoelectron spectroscopy (XPS) and MDS it was shown that O_2^- does not desorb upon annealing but dissociates and ends as a buried oxygen species below the Cs atoms [28]. The thermal activation energy of 0.8 eV is the rate limiting step for the dissociation process of the O_2^- species that leads to exoemission. This value is much lower than the dissociation energy into O and O^- as derived from the anharmonicity of the stretching vibration (3.9 eV). The dissociation must therefore proceed via additional charge-transfer into the anti-bonding orbitals of the O_2^-. This must involve the thermal activation of an electron source. Given the known response of the Cs–O system to oxygen pulses a thermal activation where O_2^- particles do not change sites can be excluded in favor of a picture where the O_2^- species diffuse on the surface and dis- sociate/de-excite on sites where electrons become available for the affinity level of the O_2^- ion [111].

Up to this point it has been sufficient to describe the kinetics with an O_2^- precursor state (A sites) and a number of exoactive B sites, while the transition from molecular A sites to atomic B sites is monitored by the exoemission. Additional experimental evidence has revealed, however, that this kinetic scheme is incomplete and has to be extended by a further step in order to account for all observations. In Fig. 29 is shown an experiment on a surface that was oxidized as in Fig. 18 and heated to 415 K. Readmission of oxygen leads again to strong exoemission in which two decay rates are observed. After switching off the O_2 supply, the current decays rapidly to zero, persumably reflecting the exhaustion of the supply of O_2^- species at the A sites. Repeated switching of the O_2

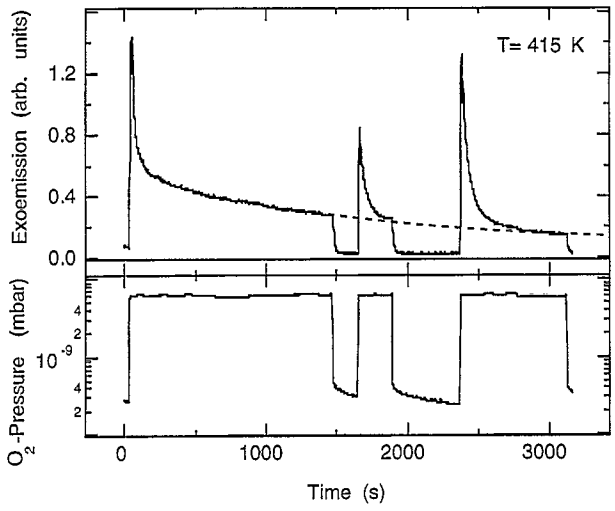

Fig. 29. Exoelectron yield from a preoxidized monolayer of Cs on Ru(0 0 0 1) at 415 K as a function of time for a varying program of O_2 interaction (see Fig. 18). From [115].

supply leads to multiple repetition of the emission, whereby the charge emitted per O_2 molecule decreases only slowly. Clearly, thermally stimulated restoration of exoactive B sites is occurring. The degree of restoration of B sites depends on the preceding O_2 exposure as well as on the duration of the interval for which the gas supply is switched off. The kinetics as shown in Fig. 29 can be simulated if a third category of C sites is introduced that is thermally populated by thermal activation of species on B sites. The complete kinetic analysis that includes the modeling of experiments at different temperatures then yields the schematic potential diagram shown in Fig. 30 for the process involved in the emission of electrons.

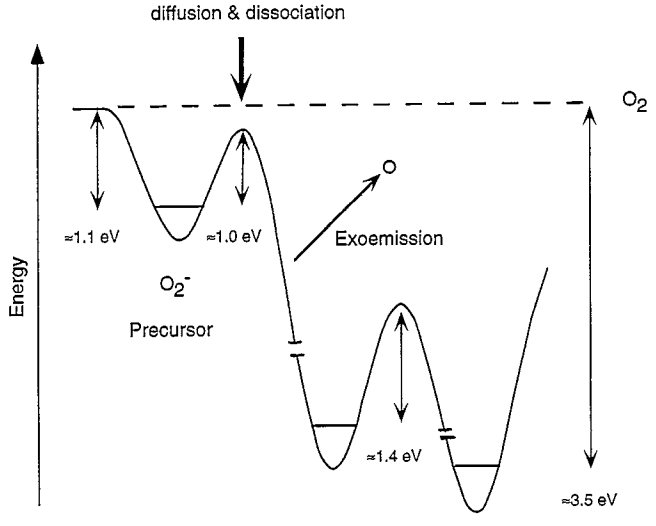

Fig. 30. Schematic potential diagram for the processes involved in the emission of exoelectrons from the oxidation of a monolayer of Cs on Ru(0 0 0 1). From [115].

These findings resemble to some extent the reports of chemiluminescence accompanying the oxidation of Al and Ti films where two time constants and partial restoration of the activity by storage of the sample in vacuum were also found [101]. This effect was tentatively attributed to the presence of two types of sites with differing efficiency for chemiluminescence.

For the case of the oxidation of Cs monolayers on Ru(0 0 0 1) it was, however, shown that the kinetics of exoemission were described by one type of transition $A \rightarrow B$, i.e. by the dissociation of O_2^- species adsorbed on a surface and by the thermal restoration of B sites $B \rightarrow C$. The results presented in this section emphasize that several thermally activated processes are involved in the formation of a Cs oxide layer on Ru(0 0 0 1) and that exoemission is a suitable tool for the exploration of the kinetics of phase transformations. However, more information is needed to properly explore the dynamics of the excitation process leading to exoemission in such systems.

4. Dynamics

The emission of non-adiabatic particles is an excellent probe for the study of adsorption dynamics. Far from thermal equilibrium, such particles probe the highest excitations in the course of a reaction. They are highly energetic and have a correspondingly short lifetime. The emission is triggered by the reaction, and timescales in the subpico second region are accessed.

This section focuses on the spontaneous reactions that lead to electron emission from metallic surfaces. These reactions do not pass any precursor on the surface and are therefore the most easily modeled. The chemical hole diving model (cf. Section 2.2.3) is used. In this model electron emission is described as the Auger de-excitation of a hole state that is injected into the electron gas. Fig. 31 recalls the situation in a dynamic correlation diagram where an empty affinity level dives below the

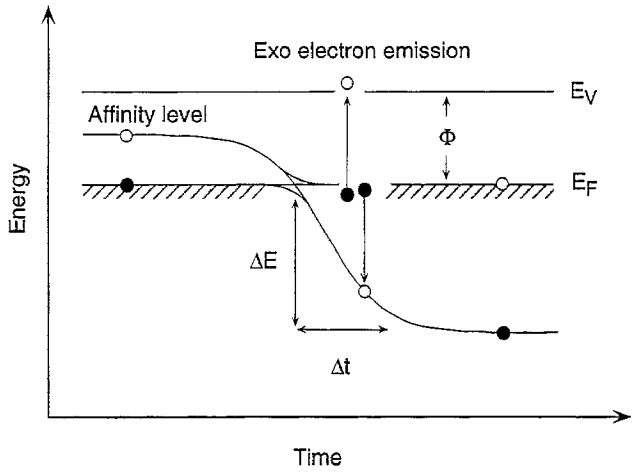

Fig. 31. Dynamic correlation diagram for the diving of an affinity level below the Fermi level E_F. When the hole injection is fast enough, electronic excitations may be created that exceed the work function Φ and lead to the emission of an Auger electron above the vacuum level E_V. From [30].

Fermi level. If it survives down to excitation energies deeper than the work function $\varepsilon_x > \Phi$ then Auger electron emission into the vacuum is possible. The ratio $\Delta E/\Delta t$ is a measure of the power dissipation in the reaction. From the energy uncertainty principle $\Delta E/\Delta t > \hbar$ the quantum mechanical limit for this dissipation power is $P < \Delta E^2/\hbar$. Typical energies for a charge-transfer of 5 eV correspond to $P < 6$ mW. However, the dissipation powers for the de-excitation of chemical energy are found to be smaller than the quantum mechanical limit by several orders of magnitude since the motion of the atoms that carry the excitation is slow compared to that of the electrons.

In Section 4.1 the model for direct dissociative adsorption is reviewed. In Section 4.2 it is shown how the energy of these particles measures the reaction enthalpy in a charge-transfer. In Section 4.3 the reaction time for the rearrangement of the chemical bonds is estimated from the probabilities of non-adiabatic particle emission. Finally the question as to how much of the free enthalpy of the reactants is released as kinetic energy of the (intermediate) products is addressed. The answer provides new insight into hot adatoms formed in the course of a reaction. Recent seeded molecular beam experiments by Böttcher et al. [29,30] and Hellberg et al. [37] will be described. It turns out that dissociated molecules become hotter at surfaces than in the gas phase – a fact that is exploited in heterogeneous catalysis.

4.1. Harpooning and direct dissociation of halogens and oxygen on alkali metals

The class of gas – solid reactions with direct dissociation of diatomic molecules can be divided into two types. There is the harpooning type in which the key role is played by the charge-transfer and where non-adiabatic particle emission is observed, and there is the non-harpooning type in which precursor free dissociation occurs, as for example, in the case of H_2 on Cu [121] or H_2 on Al (110) [122]. The concept of harpooning was originally developed for gas phase reactions [13,14,45] and then successfully applied to gas/solid reactions [1,135–138,141]. Gadzuk [137] describes the colorful terminology of harpooning being derived from the image of the electron (harpoon) thrown out from th e metal (the Pequod) to the approaching molecule (Moby Dick) which is then reeled in by the Coulomb force.

For the reaction of alkali metal surfaces with highly electronegative diatomic molecules X_2 such as O_2 and the halogens, the following charge-transfer reaction leading to non-adiabatic particle emission occurs [26,27,30,37]. The reaction may be divided into two steps: (i) an acceleration phase and (ii) a non-adiabatic de-excitation phase in which particles are emitted, as negative ions and/or electrons and photons. The acceleration takes place after harpooning $X_2 \rightarrow X_2^-$ in the image potential. This triggers dissociation in which negative ions X^- may escape the surface [26,55,56] and in which de-excitation of the atomic $X(p^5)$ species with one hole in the valence p-shell into the closed shell $X(p^6)$ species may lead to exoelectron emission [27,37,51] and/or chemiluminescence [1].

In Fig. 32 the mechanism is sketched for oxygen and chlorine. The adsorption starts with the approach of a thermal X_2 molecule to the metal surface. The image force lowers the affinity level of the X_2 molecule, which resonantly ionizes as soon as it crosses the Fermi level [123]. As outlined by Hellberg et al. [37] (cf. Section 2.1), the verticel affinity $E_A^V(X_2)$ determines the harpooning distance. Now the X_2^- molecule is accelerated by its image field to the surface. These vertical electron affinities for O_2 and Cl_2 differ considerably where it is negative for oxygen, it is positive for chlorine. While X_2^- halogens immediately start to dissociate and become exoactive, O_2^- ions are still bound as a molecular ion that only starts to dissociate after a second electron transfer into the anti-bonding

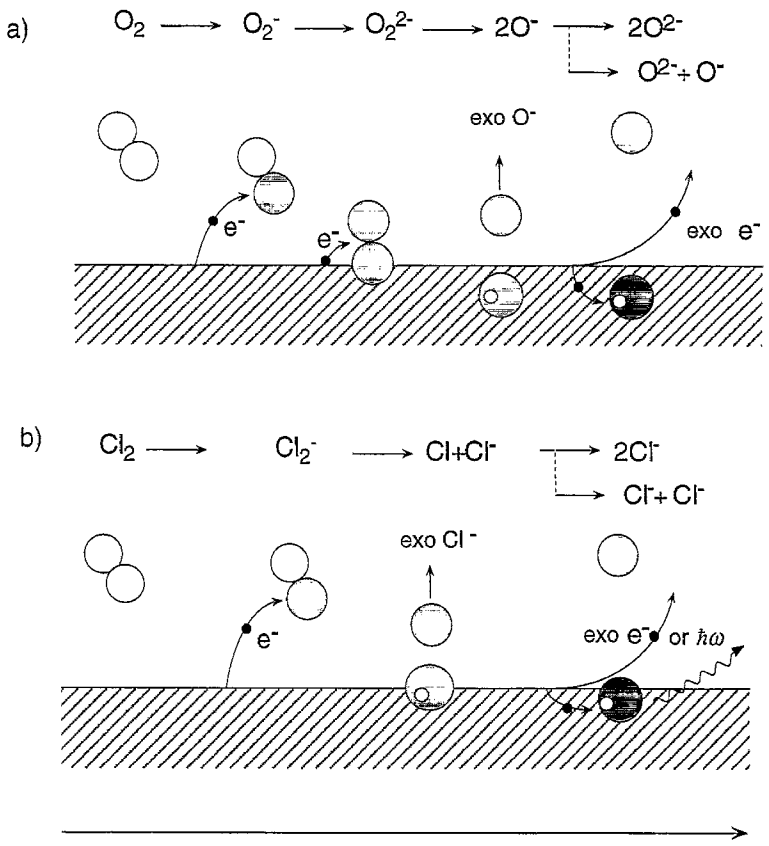

Fig. 32. Model for harpooning and direct dissociation for oxygen (a) and halogens (b), respectively. The molecules approach the surface adiabatically and are resonantly ionized (harpooned). The molecules further accelerate and dissociate while negatively charged ions may escape the surface. The highly excited $X(p^5)$ dissociation intermediates may de-excite non-adiabatically by (a) the emission of exoelectrons or (b) by the emission of exoelectrons or photons.

$1\pi_g$ orbitals. After the second electron transfer ($O_2^- \rightarrow O_2^{2-}$) the hot O_2^{2-} species bursts into two O^- fragments.

If the momentum of one of these fragments, X^- and X^* in the case of the halogens, and the two O^- in the case of oxygen, is large enough and directed away from the surface, it may escape the metal. The dissociation process will on the other hand leave $X(p^5)$ species on the surface. This is a high excitation of the $X(p^6)$ ground state that is reached after a complete reaction. In a one electron picture the affinity level of the $X(p^5)$ will start to dive to its ground state position at the $X(np)$ binding energy (see Fig. 31). The observation of electron emission implies that this hole injection process, i.e. the X_2 dissociation, is so fast that some $X(np)$ holes may dive deeper than the work function and cause the emission of Auger electrons. In the case of oxygen, where the de-excitation happens due to the negative vertical electron affinity and due to the correspondingly low harpooning distance at a site with high electron density, it is expected that the O(2p) hole does not live long enough for substantial production of light [33]. In the case of the halogens, however, the early harpooning produces neutral $X(p^5)$ species at a relatively low electron density that may, with the emission of light, de-excite to the $X(p^6)$ ground state ions.

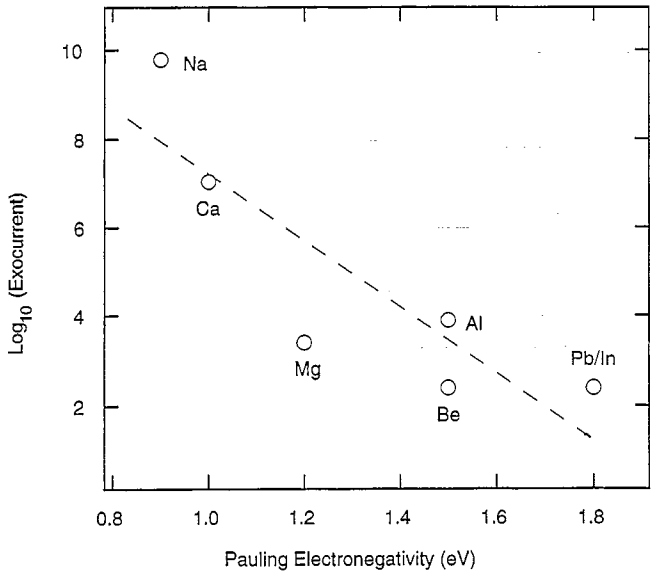

Fig. 33. Correlation of the logarithm of the exoelectron yield with the Pauling electronegativity of the substrate after abrasion with a stainless steel brush in high vacuum. Data from [91].

4.2. De-excitation energy

The probability for exoelectron emission depends on the difference between the electronegativities of the adsorbing molecule and of the substrate. This already indicated the early investigation of Lohff and Raether [91], who studied the after-emission from in situ abraded metals, and is summarized in Fig. 33. The initial emission probability is correlated on a logarithmic scale with the Pauling electronegativity $\chi_P = \frac{1}{2}(I_p - E_A)$ where I_p is the ionization potential of the substrate and E_A the electron affinity of the adsorbate. The rough trend ($Y \propto e^{-\chi_P/b}$ with $b = 0.06$ eV) reflects the strong dependence of the emission probability on the difference in electron affinity between the reaction partners.

The relation between the released energy and the emission probability can be further explored by measuring the energy of the emitted electrons or photons. The high energy cut off, measured relative to the Fermi level, provides a lower boundary for the released energy in the charge-transfer reaction leading to electron emission, while the low energy cut off provides a measure of the work function of the substrate. In most cases the electrons emerge just at the vacuum threshold and therefore it is the work function, correlated as it is with the electron affinities [124,125], which most strongly affects the emission probabilities.

In the Kasemo picture, in which electron emission originates from the de-excitation of an empty affinity level at ε_A below the Fermi level [57], the electron emission probability will depend on the work function, which must be smaller than ε_A. For positive excess energies $(\varepsilon_A - \Phi) > 0$) it can be shown that the yield follows a power lay $Y \propto (\varepsilon_A - \Phi)^\kappa$. The exponent κ depends on the model that is applied (see Sections 2.2.1 and 2.2.3). Prince and coworkers [59] determined ε_A values for the reaction

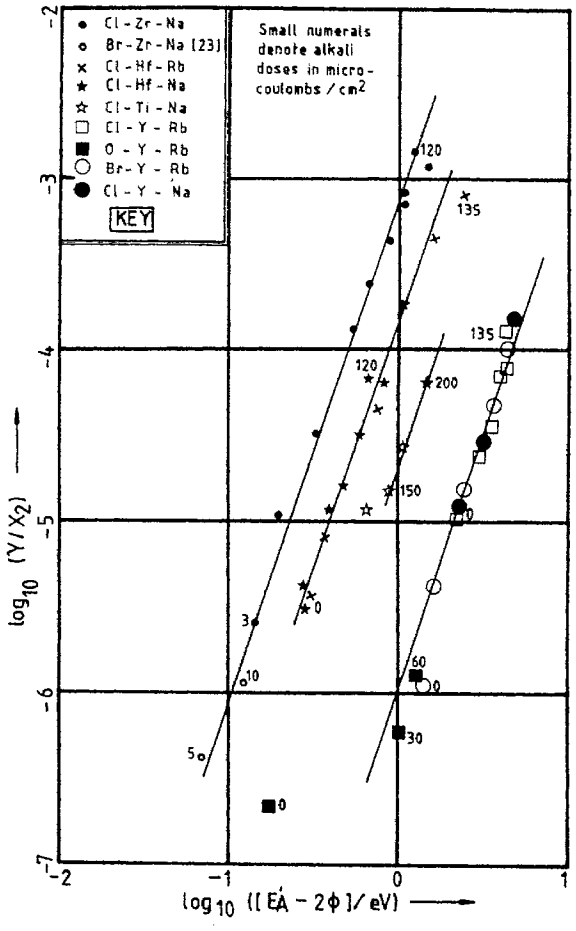

Fig. 34. Master diagram showing cubic relationship between exoelectron yield and excess energy ($E'_A - \Phi$). From [85].

of halogens with metallic surfaces from the knowledge of the work function and from the assumption of a cubic dependence of the yield, i.e. $\kappa = 3$. Fig. 34 shows the systematic analysis of Cox et al. [85]. It is a log–log master diagram that summarizes the results. The electron yields from the exposure of X_2 (X = Cl, Br, O) to substrates such as Ti, Zr, Hf and Y were measured as a function of the work function, which was varied with submonolayers of Na and Rb alkali metals. The ratio of electron to negative ion currents was determined by the application of a magnetic field which deflected the ions only slightly while returning electrons to the sample. Note that in Fig. 34 the E'_A correspond to the effective affinity as measured from the vacuum level and thus yield is plotted versus $\log(E'_A - 2\Phi)$. In the rest of this text the effective affinity ε_A is referenced with respect to the Fermi level, i.e. $\varepsilon_A = E'_A - \Phi$. The E'_A values for the determination of the excess energy were compared with the electron affinities of the atomic constituents of the adsorbates in the gas phase $E_A(X)$, i.e. $E'_A = E_A(X) + \chi$. The difference between the two $\chi = E'_A - E_A(X)$ was assumed to be the same for all reactions and was determined to be 4.2 eV. The energy reference in the picture of Cox et al. is the

vacuum level and not the Fermi level. This implies, for example, that the maximum available excitation energy ε_A depends on the work function. χ was attributed to the image potential contribution, i.e. the average down shift of the affinity level. From this the exoelectron yield was found to be universal up to a substrate related pre-cubic factor and to depend only on the atomic affinity $E_A(X)$ of the adsorbate and on the work function. As can be seen in Fig. 34 the pre-cubic factor varies from Zr to Y by a factor of 400. The authors claim that it does not seem possible to give a qualitative explanation for this observed trend in the pre-cubic factor from metal to metal. They state that the effective affinity E'_A of the incoming atom might behave differently on different metals. This is very likely since the image potential contribution does not have to be a constant for all metals and adsorbates. This is emphasized, for example, by the differences between heats of formation per transferred electron for the different systems.

The interpretation of Cox et al. is based on the cubic law [59], i.e. on a static picture that implies the sudden creation of a hole below the Fermi level. This assumption may be sufficient to explain the observed trends, but it will not provide a quantitative description as soon as the timescale of electronic motion is faster than that of the atom that injects the affinity below the Fermi level.

For the oxidation of Li the same concept of fitting a power law $Y \propto (\varepsilon_A - \Phi)^\kappa$ to the emission probabilities was applied [51]. In this study the work function changes could be directly determined from the low energy cut off of the exoelectrons. Furthermore in the first oxidation step, which is assigned by spectroscopic methods to the embedding of O^{2-}-like ions below the surface, i.e. to the formation of Li_2O, the work function strongly decreases from 2.9 to 1.8 eV. The exponent κ was left as a free fit parameter and a value $\kappa = 5.8 \pm 1.5$ was found (see Fig. 35). This value of κ does not support a static picture, i.e. there is no cubic dependence of the yield as a function of the excess

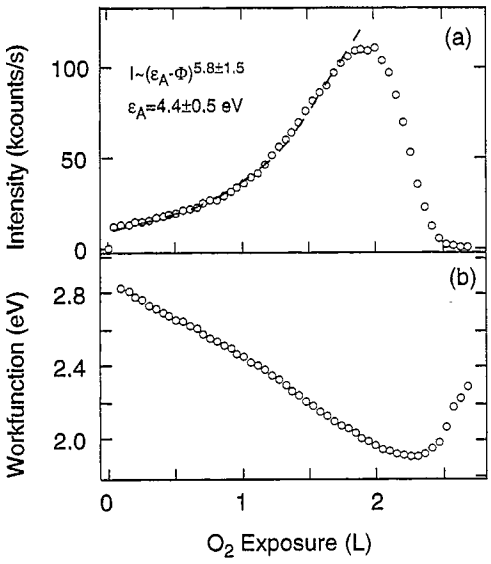

Fig. 35. (a) Yield of exoelectrons from 2 ML Li on Ru(0 0 0 1) at 300 K exposed to 10^{-6} Pa O_2 as a function of oxygen dose (1 L = 1.3×10^{-4} Pa s). The increase in intensity is fitted to a power law $I \propto (\varepsilon_A - \Phi)^a$. (b) Work function as directly determined from the kinetic energy distribution of the exoelectrons. The initial value of Φ was determined from UPS. From [51].

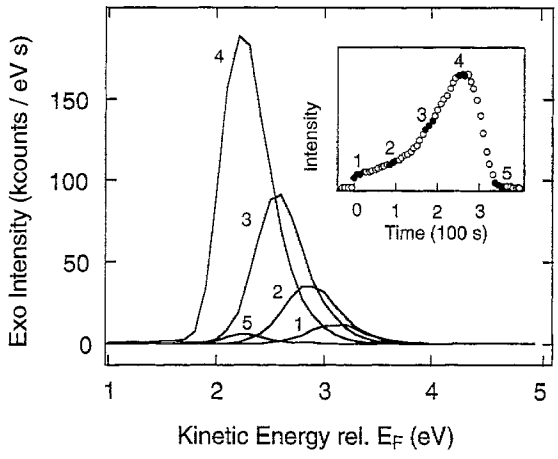

Fig. 36. Kinetic energy distributions of exoelectron emission from Li recorded with an instrumental resolution of 500 meV. The inset identifies the spectra with the corresponding kinetics. Note that the maximum kinetic energy is below 4 eV with respect to the Fermi level. From [51].

energy. The exponent as determined from the experiment is influenced by progressive oxidation during the experiment, which continuously reduces the fraction of the surface that is exoactive. But even if an exponential decrease with exposure of this fraction is taken into account, the experimental value of 5.8 ± 1.5 cannot be explained by the static picture, in which it is supposed that the empty affinity level is suddenly injected at ε_A. If, however, there is a finite probability that the hole will decay as soon as it is created and starts its dive in the Fermi sea down to ε_A then a larger exponent can be readily explained. The ε_A value as determined from the experiment gives, however, a measure of the energy released in the reaction. In the case of the oxidation of Li ε_A was found to be 4.4 ± 0.5 eV.

If the data in Fig. 35 are fitted to a cubic law with the vacuum level as reference $Y \propto (E'_A - 2\Phi)^3$ we find for E'_A a value of 7 ± 0.1 eV. If the exponent is left as a free parameter we find $\kappa = 3.5 \pm 1$ which is compatible with the cubic law. In the model of Prince et al. [59] a constant image potential shift $\chi = E'_A - E_A(O) = 5.6$ eV follows. This is larger than the value of Cox et al. [85] (4.2 eV). There is, however, further evidence that the Fermi level is the point of reference for the Li + O_2 reaction. First, the exoelectron energy spectra do show a constant high energy cut off that is independent of the work function, as can be seen in Fig. 36. In the picture of Cox et al., the high energy Auger cut off should shift to higher energies with lower work function. In the regime of Li_2O formation the O 2 p binding energy as measured with ultraviolet photoelectron spectroscopy (UPS) does not shift with respect to the Fermi level. The second argument that favors the Fermi level reference is the coincidence between the experimentally determined [51] and the calculated [27] de-excitation energies of 4.4 ± 0.5 and 4.5 eV, respectively. The cluster calculations were performed in the framework of a local spin density approximation (LSDA) formalism. The calculations yield potential energy surfaces for cluster ground states and for excited states that were determined as ground states with spin symmetry constraints. In Fig. 37 three of these potential energy surfaces are shown for O, O^- and O^{2-} oxygen species as they approach a Li cluster. The Li (6.2) cluster mimics an ideal bcc (1 0 0)

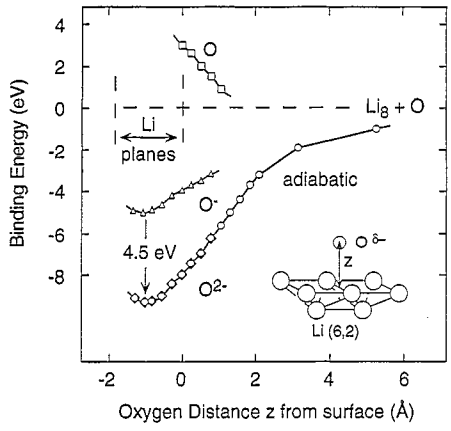

Fig. 37. Total energy calculations within the LSDA formalism with charge and spin constraints. A cut across the potential energy surfaces of O (squares), O^- (triangles) and O^{2-} (diamonds) is shown on the surface normal along the bridge site (see inset). The oxygen penetrates below the surface and ends up in a closed shell O^{2-} configuration. The de-excitation energy between O^- and O^{2-} below the surface corresponds nicely with the observed maximum de-excitation energy of exoelectrons. Every symbol stands for a self-consistent calculation. Data from [51].

surface with a lattice constant of 3.45 Å, and with six atoms in the first and two in the second layer. The lateral reaction coordinate was chosen for the oxygen approach on the bridge site as can be seen in the inset to Fig. 37. It shows that on the adiabatic ground state potential oxygen atoms penetrate the surface as charged species. The energy minimum is the closed shell O^{2-} ion between the Li layers. This is in accordance with an effective medium theory [48] in which the electron density with the maximum binding energy of oxygen is close to that of Li. Since Li has the highest electron density of all alkali metals, oxygen should penetrate below the surface of all alkali metals. The penetration of oxygen below the first layer was also confirmed by complementary MDS and by UPS. It is further supported by the observation that the work function decreases with progressive formation of Li_2O-like surface oxides [51]. The LSDA calculations indicate that the de-excitation energy from O^- into O^{2-} is 4.5 eV. This matches with the experimentally derived maximum de-excitation of 4.4 ± 0.5 eV. Therefore the model for exoemission in the $Li + O_2$ case was ascribed to the Auger de-excitation of a hole on the O^- ion, leading to the O^{2-} ground state. In Section 4.3 the modeling of the dynamics, i.e. the temporal evolution of the hole on the O^- ion, will be described. The above findings confirm that the model proposed on the basis of O^- emission in the $Cs + O_2$ reaction [26] is appropriate for the interaction of oxygen with clean alkali metal surfaces.

The reaction model as described in Section 4.1 includes the intermediate formation of O_2^{2-}, which dissociates into two O^- ions. The notation of discrete charge states allows a clear labeling of the different steps. It is a simplification and merely describes the symmetry as expressed for example by spin analysis.

The formation of O_2^{2-} was debated by Wang [36] who excluded the formation of O_2^{2-} on grounds of electrostatic arguments. There are no experiments at hand that can decide this issue. There are, however, arguments in favor of the O_2^{2-} hypothesis: The same LSDA formalism with spin constraints as described above indicated for Li(6, 4) $+ O_2$ clusters "diamagnetic", i.e. closed shell O_2^{2-}-like oxygen, without any appreciable barrier for dissociation [27] and the O_2^{2-} ion may be

screened by the electrons of the surface and have a similar configuration to that of oxygen in alkali peroxides (A_2O_2).

4.3. Reaction time

Provided that there is enough free enthalpy ΔE in order to surmount the emission threshold the reaction time Δt, i.e. the time for the rearrangement of chemical bonds governs the non-adiabatic yield. For large non-adiabatic yield Δt should be as short as possible. In Fig. 31 the situation leading to the emission of electrons is depicted in a dynamic correlation diagram in which the affinity level of the reacting species and the levels of the substrate are shown as a function of time. Normally the affinity level is resonantly ionized as soon as it dives into the Fermi sea. For strong and fast reactions, however, the empty affinity level may survive an injection deeper than the work function and de-excitation via Auger electron emission is enabled. Since these electrons get energy and momentum during the reaction the probability of their emission is a direct consequence of the dynamics of the process. It is therefore an inversion (reverse) problem to derive the reaction time from these probabilities.

A proper description of the quenching of these excitations gives the ratio between the adiabatic and the non-adiabatic reaction branch as a function of the reaction time Δt (the time the system requires to dissipate the energy ΔE). A comparison with experimentally observed emission probabilities enables the derivation of the reaction time and gives a measure of the maximum energy dissipation $\Delta E/\Delta t$ [33]. Within this chemical hole diving model exoelectron emission probabilities were calculated for the simplest situation, i.e. a metallic jellium surface [33] for which problem electron gas theory can be used [126]. The reaction leading to electron emission is described as a hole state (derived from an affinity level on a reacting particle) that dives into the Fermi sea (see Fig. 31). The survival of this hole as a function of time and energy and the probability of its decay via the emission of an Auger electron into the vacuum were calculated. This emission probability is mainly determined by the power dissipation $\Delta E/\Delta t$ and by the work function. The time Δt is expressed in units of the hole lifetime τ_ε at the final binding energy of the affinity level (cf. Section 2.2.3). For the case of the reaction of oxygen with alkali metals the calculated time Δt corresponds to the dissociation time of O_2^{2-} into two O^{2-} with an O 2p binding energy at ΔE.

In Fig. 38 the calculated emission probabilities are shown as a function of the ratio between the work function and the position of the affinity level after the reaction (i.e. at the O 2p binding energy ε_A). The solid lines are the probabilities for different reaction times expressed in terms of hole lifetimes τ_ε of the affinity level at ε_A. Reaction times of 140 ± 20 and $70 \pm 10\ \tau_\varepsilon$ are found for Li and Cs, respectively. The broadening, i.e. the absolute value of $\tau(\varepsilon_A)$, affects the probabilities only in second order. From the width of the energy distribution of the exoelectrons, τ_ε can be estimated and in the case of Li a value of ≈ 1 fs was found [33]. This indicates that the dissociation time of O_2 is of the order of molecular vibration periods. The reaction of O_2 with Cs appears to be faster. There is no contradiction with the fact that the heat of formation for Cs_2O is smaller since the O 2p hole lifetime of Cs is larger than that of Li, because the electron density is smaller in the case of Cs. According to Pines and Nozières the hole lifetime in a dense electron gas ($r_S < 1$) is proportional to the plasmon frequency [126]. If we normalize the reaction times from above with the square root of the electron density of Cs ($0.91 \times 10^{28}\,m^{-3}$) and Li ($4.7 \times 10^{28}\,m^{-3}$) we find reaction times of 140 ± 20 and $160 \pm 20\ \tau_\varepsilon$ (Li) for Li and Cs, respectively.

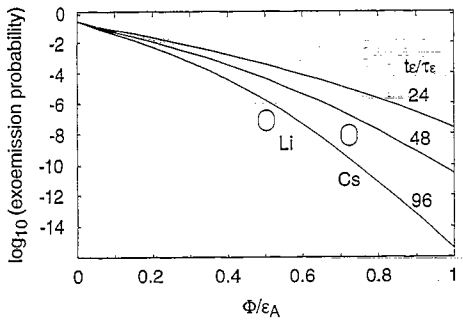

Fig. 38. Comparison of experimentally observed exoelectron emission yields at the beginning of the oxidation of alkali metal films with predictions of the chemical hole diving model [33]. The apparently longer reaction time t_e/τ_ε for Li can be understood with the shorter electron–hole pair lifetime τ_ε in Li compared to Cs.

In order to cross check these results chemiluminescence experiments were performed in the $Li + O_2$ reaction. Fig. 39 shows the emission of visible light from (a) the reaction of O_2 with two monolayers of Li on Ru (0 0 0 1), and (b) from Ru (0 0 0 1). There is a very weak signal that corresponds to less than 10^{-10} visible photons per O_2 molecule and no distinction can be made between signals from the reaction of O_2 with Li and that from the clean Ru (0 0 0 1) crystal. This yield was taken as an upper limit for chemiluminescence. As can be seen in Fig. 39(c), traces of a monolayer of Li on the photomultiplier window induced a multiple of the light emission from the metallic

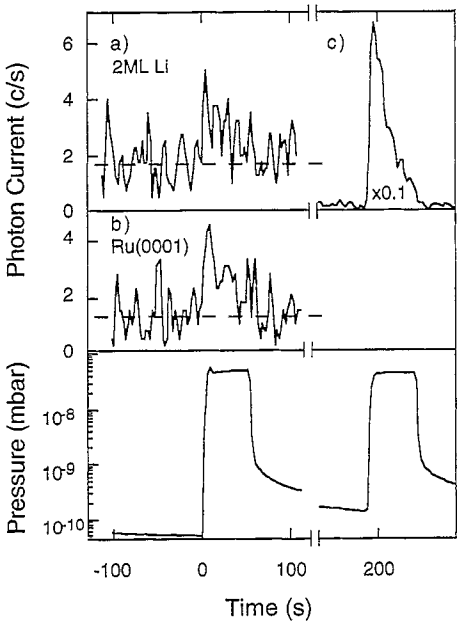

Fig. 39. Photon ($300 < \lambda < 800$ nm) emission during the oxidation of (a) 2 ML of Li on Ru, (b) clean Ru(0 0 0 1) and (c) from the photomultiplier window with traces of a monolayer of unoxidized Li adsorbed. The bottom panel shows the corresponding oxygen exposure. From [51].

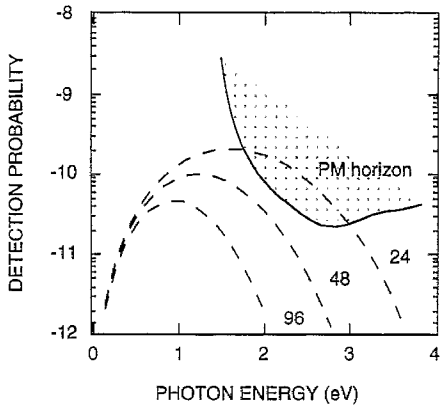

Fig. 40. Chemiluminescence spectra as expected from the chemical hole diving model [33] for reaction times of 24, 48 and 96 $t_\varepsilon/\tau_\varepsilon$. The current "photomultipier-horizon" shows the sensitivity of the experiments of Ref. [51]. The absence of significant chemiluminescence in the reaction of Li with O_2 is therefore consistent with reaction times $> 50\ t_\varepsilon/\tau_\varepsilon$.

samples. This means that the light shown in Fig. 39 (a) and (b) might stem from insulalting contaminations in the subpercent range.

The chemiluminescence spectra were calculated from the chemical hole diving model [33] and compared with the electron emission probability. Assuming that at the energy ε_A there is a branching between photon and electron de-excitation (note not electron emission) η of 10^{-6} (asuming optical lifetimes of 10 ns and electronic lifetimes of 10 fs), we find photon emission probabilities of 0.010, 0.005 and 0.002 η for $t_\varepsilon/\tau_\varepsilon = 24$, 48 and 96, respectively, where $t_\varepsilon/\tau_\varepsilon$ is the hole diving time down to ε_A. These spectra are shown on a logarithmic scale in Fig. 40, where the sensitivity of the measurement of Ref. [51] is indicated with the photomultiplier horizon.

These probabilities cannot easily be measured, since a large portion of the spectra is in the infrared where the sensitivity for observation decreases. Within the proposed model the absence of chemiluminescence ($< 10^{-10}$ 600 nm photons/O_2) is therefore compatible with the observed electron emission probabilities.

4.4. Intermediate velocities of dissociating atoms

Most chemical reactions have to be activated in order to proceed. Normally the activation energy comes from the heat bath in which the reaction takes place. If the heat of formation is, however, released to single reactants intermediate hyper-thermal products may be produced. These particles may induce further reactions with activation energies exceeding $k_B T$, where T is the temperature of the heat bath. Such situations are met in heterogeneous catalysis where for example the heat of adsorption is released to single atoms or molecules, which dissipate energy until thermal equilibrium is reached.

In order to study the restoration of thermal equilibrium, scanning tunneling microscopy experiments were performed. The positions of atoms of dissociated molecules were recorded after the reaction on the substrate [127,128]. These beautiful experiments by Wintterlin et al. give an a posteriori insight into the mechanism of chemical energy dissipation. For oxygen adsorption on

Al(1 1 1) Brune et al. found single oxygen atoms after the reaction. Even for the lowest oxygen exposures no pairs of oxygen atoms could be associated. Thus the authors gave a lower limit of 80 Å for the separation between oxygen atoms before they came to rest on the substrate. This is evidence that hot adatoms are formed in the course of a reaction. In a subsequent study of the oxidation of Pt (1 1 1), pairs of oxygen atoms could be identified after the reaction. In this case the oxygen atoms appear to be separated on average by two lattice constants. As well as allowing the determination of the activation energy for diffusion this observation is also an indication that non-thermal processes take place during dissociation [128]. The average separation distance of two lattice constants is compatible with molecular dynamics simulations and with known dissipation mechanisms [129–131]. In this light the dissociation and dissipation mechanism of O_2 on Al (1 1 1) is not fully understood. The experiment might in fact hint at a dissociation mechanism with a cannon ball trajectory [129,132].

The study of non-adiabatic particles is another class of experiments that accesses the effective temperatures of intermediate reaction products. In complement to the above-mentioned statistical evaluation of spatial distributions of reaction products by scanning tunneling microscopy [127,128] the intermediate velocities of the involved particles directly affect the non-adiabatic particle yields [29,30,33,35,37,38,133] and therefore give direct insight into the reaction dynamics.

Here the oxidation of alkali metals serves as a model case for direct dissociative adsorption. The observation of O^- emission during the reaction of O_2 with Cs leads to the proposition that intermediate O_2^{2-} formation triggers dissociation [26]. It also suggested dissociative adsorption in the unfavorable normal orientation of the molecular axis with respect to the surface. For the case of Li the same reaction path was corroborated by means of total energy calculations [27] (cf. Section 4.1): (i) The neutral O_2 molecule is harpooned in front of the surface ($O_2 \rightarrow O_2^-$). (ii) The O_2^- molecule accelerates to the surface and picks up a second electron ($O_2^- \rightarrow O_2^{2-}$). (iii) This O_2^{2-} intermediate dissociates into two O^- species ($O_2^{2-} \rightarrow 2O^-$) that may further de-excite ($O^- \rightarrow O^{2-}$) into the closed shell O^{2-} ground state (see Fig. 31).

Böttcher et al. [29] first demonstrated that rising the mean velocity of O_2 molecules impinging onto a Cs surface has a strong effect on the yield of exoelectrons. Fig. 41 shows the intensity of exoelectrons as a function of O_2 exposure for different kinetic energies of the impinging molecules. The data for translational energies $E_{trans} = 0.12$ and 1.25 eV were obtained with different seed gas compositions but with identical nozzle temperature (720 K) and hence identical population of the vibrational levels. The difference in the yield of exoelectrons has therefore to be attributed solely to the variation of the translational energy. This trend is continued with the curve for $E_{trans} = 0.06$ eV (nozzle temperature 300 K) where the yield is still somewhat lower, but by no means reflects the associated pronounced difference in the concentration of vibrationally excited molecules. At 300 K 0.3% of the molecules are vibrationally excited ($n_v > 0$) while 10% are excited at 720 K. This means that the variation of the yield of exoelectrons is dominated by the translational energy of the O_2 molecules while their vibrational energy is of (if at all) little or no influence.

The effect of the translational energy on the exoelectron yield is most pronounced in the early stages of oxidation where an increase by up to about two orders of magnitude is observed, while in the range of the maximum intensity (= work function minimum) only a weak variation is observed. This difference is associated with the different surface chemistry and mechanisms of exoelectron emission: At the metallic Cs surface an O_2 molecule initiates a cascade of various ionizing processes which can contribute to spontaneous exoemission. In later oxidation stages a weakly bound

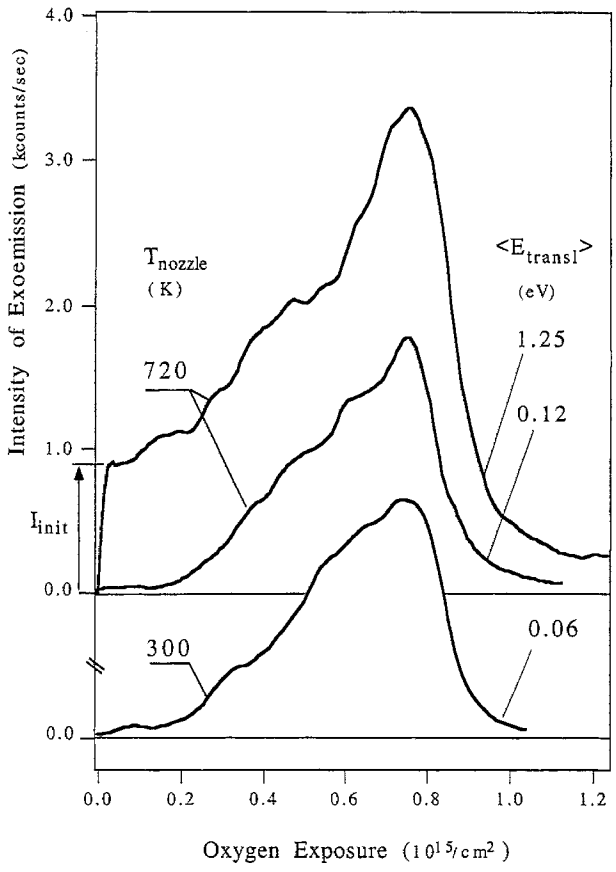

Fig. 41. Exoemission as a function of O_2 exposure. The maximum emission corresponds to about 2.6×10^{-4} Pa s O_2 exposure. The initial intensity I_{init} strongly depends on the translational energy but not on the temperature of the nozzle. From [29].

metastable peroxo O_2^- species is formed on top of the partly oxidized surface. The transformation of this may lead to exoemission too [28]. Consequently the yield of exoelectrons in this range depends on the sample temperature but is only weakly affected by the kinetic energy of the impinging molecules.

In the following discussion we will concentrate on the initial stage of oxidation where the exoelectron yield is independent of surface temperature, but is strongly affected by the translational energy, signaling that exoelectron emission results from a direct impact process.

As can be shown from the model in [33] or from other earlier models describing non-adiabatic transitions [69,70,134], the probability of a non-adiabatic reaction is proportional to $e^{-v^*/v}$ where v is the velocity during the reaction and v^* describes the dynamics of the excitation/de-excitation process.

The exoelectron yield is proportional to $e^{-\Delta t/\tau_0}$ where Δt is the reaction time and τ_0 is a characteristic time which describes the quenching of the excitations that may lead to exoemission (cf. Fig. 15). On writing formally $\Delta E/\Delta t = v\nabla E$ where ∇E is the energy gradient of the affinity level along the

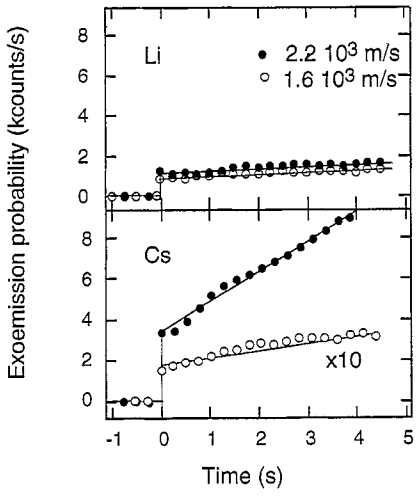

Fig. 42. Initial probabilities for exoelectron emission from (a) Li and (b) Cs for two different velocities of the impinging O_2. From [30].

reaction coordinate and v the corresponding velocity, it becomes evident that the non-adiabatic yield is higher for larger v. Most non-adiabatic reaction products are created in the hottest stage of the charge-transfer cascade, i.e. in the $O_2 \rightarrow 2O^{2-}$ process. For the case of the oxidation of Li the reaction step $O_2^{2-} \rightarrow 2O^- \rightarrow 2O^{2-}$ has been assigned to the exoelectron emission and a time Δt of the order of 100 fs was found for the dissociation of O_2^{2-} into two O^{2-}. This is in the range of molecular vibration periods [33,51].

Fig. 42 shows the initial exoemission from thick films of Li and Cs versus the time of O_2 exposure for two different molecular impact velocities [30]. While the emission from Li does not increase greatly a strong increase is found for thick Cs layers, just as was found for a monolayer of Cs [29] (see Fig. 41).

Fig. 43 shows the logarithm of the initial emission probability versus the inverse normal velocity $1/v_\perp(O_2)$ for the oxidation of Li and Cs. The full symbols represent the total emission probabilities of negatively charged particles. For the case of Cs the fraction of O^- ions as estimated from magnetic stray field experiments is indicated with open circles. The O^- yield from the Li + O_2 reaction is even lower [51].

The characteristic velocities v^* cannot be straightforwardly determined from a plot of $\ln(P_{exo})$ versus $1/v_\perp$ (see Fig. 43) where $v_\perp$ is the normal velocity of the impinging O_2 molecules since $v_\perp$ is not necessarily the velocity during the reaction that yields the excitation of an electron into the vacuum. The reaction itself provides additional velocity due to the chemical interaction into the coordinate for the dissociation. This is supported by the fact that even for thermal O_2 molecules the non-adiabatic electron emission does not vanish [27,51]. Furthermore it cannot be expected that all momentum of the impinging O_2 will couple into the reaction coordinate. The expression for the reaction velocity v should read as $v = \alpha(v_\perp + v_c)$, where v_c is the additional velocity due to the chemical interaction and α is an efficiency number ($\alpha \leq 2$) for the coupling of the velocity of the O_2 molecule into the dissociation coordinate (if all the momentum of the O_2 molecule is transferred to one O^-, then $\alpha = 2$ is expected) (cf. Section 2.2.2). An averaging over a random orientation

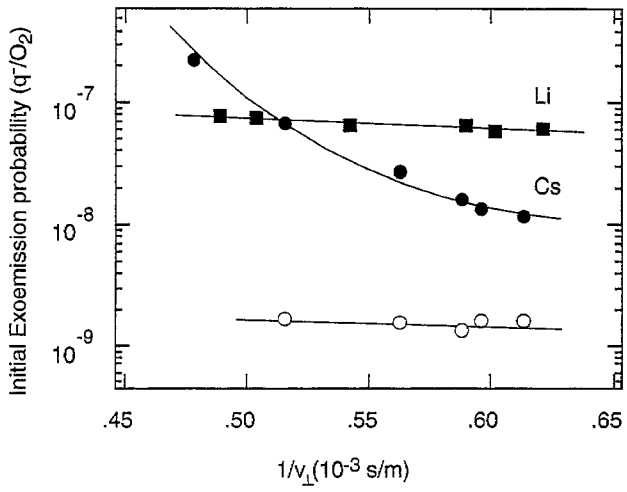

Fig. 43. Logarithmic plot of the initial exoemission probability versus $1/v_\perp$ (O_2) for Cs and Li, respectively. The open circles denote the intensities of ions emitted from a Cs surface as estimated from magnetic stray field experiments. The solid lines are guides to the eye. From [30].

multiplies α by a factor of 0.5. For $v_\perp/v_c \ll 1$ the emission probability should be unaffected from $v_\perp$ and for $v_\perp/v_c \gg 1$ the probability exponent would increase as $v^*/\alpha v_\perp$.

The data for Li in Fig. 43 therefore suggest that the velocity v_c due to the reaction is larger than 2.1×10^3 m/s since the non-adiabatic yield is almost independent of $v_\perp$ in the experimentally accessible range.

In the case of Cs the experiment accesses the transition into the regime where the initial molecular velocity dominates the velocity increase due to the chemical interaction and a strong increase in the electron yield above a velocity $v_\perp$ of 1.6×10^3 m/s is observed. Below this velocity the exoemission levels off at a probability of about 10^{-8} q/O_2. The threshold velocity may be taken as a measure for the velocity gain v_c. This explains why no threshold is observed within the experimentally accessible molecular velocities for Li since the heat of formation for Li_2O exceeds that for Cs_2O by a factor of 2 (cf. Fig. 14). The crossing of the emission probability of Cs with that of Li does not imply a shorter absolute dissociation time for O_2^{2-} on Cs – which would contradict heat of formation arguments – but it indicates that the reaction time expressed in terms of hole lifetimes becomes shorter for Cs than for Li. This is in line with the fact that the hole lifetime in a dense electron gas scales with the square root of the electron density [126]. It is nevertheless tempting to attribute the threshold to the opening of a new non-adiabatic channel. The data in Fig. 43 rule out ionic emission. The $O_2^- \rightarrow O_2^{2-}$ transition is another possible candidate. This is, however, unlikely since the molecular affinity level does not dive as deep into the Fermi sea as does that of the atom and thus the non-adiabatic yield from molecular de-excitation should be small. From the strong increase of the non-adiabatic yield for $v_\perp > 1.6 \times 10^3$ m/s an upper limit for v_c is derived and from the slope we obtain a value for v^*/α of 2.2×10^4 m/s. The resulting ratio $v^*/\alpha v_c > 14$ from the experiment can be compared with theory without knowing the hole lifetime. The hole diving model [33] gives a value of 7 ± 2 for v^*/v_c. This indicates a rather high efficiency α for the coupling of v_c into the reaction coordinate. Finally it is

worth emphasizing here that the velocity v_c is compatible with the energies indicated by the emission of negative ions, for which process an effective temperature of $\sim 6kT$ (160 meV) was found [26].

In a recent paper Hellberg et al. [37] also reported non-adiabatic yield dependencies as a function of the impact velocities of the molecules. They studied the reaction of chlorine Cl_2 with potassium K. From these and earlier findings [1,44,49,57] a model for the dissociative adsorption of halogens on alkali metals can be derived (cf. Section 4.2): (i) The neutral molecule is harpooned in front of the surface ($Cl_2 \rightarrow Cl_2^-$). (ii) The negative molecule accelerates in the image field and starts to dissociate ($Cl_2^- \rightarrow Cl + Cl^-$) where (a) the de-excitation ($Cl \rightarrow Cl^-$) may proceed with the emission of a photon [1] or (b) an electron [37] and/or (c) where Cl^- ion may escape the surface [55,56] (cf. Section 4.1). In comparison with the model for the reaction of O_2 with alkali metal surfaces the higher affinity of the halogens induces earlier harpooning, further away from the surface, in an environment with lower electron density. As a consequence the non-adiabatic particle yields are much higher.

For a Cl_2 velocity of 450 m/s Hellberg et al. found a yield of 8×10^{-4} negative particles per impinging Cl_2 molecule. They attributed it to electrons, which conflicts with the data of Trowbridge and Herschbach [55] who found a yield of 2.3×10^{-4} for Cl^- emission and negligible ($< 10^{-5}$) electron emission in the $Cl_2 + K$ system. Irrespective of the actual nature of the negative particles the yield is expected to increase with higher velocities of the impinging molecules. Since the emitted electrons and ions are expected to be created in the same stage of reaction, i.e. after image acceleration in the course of the Cl_2^- dissociation, the same semi-empirical model described above may be applied and relevant dynamical reaction parameters may be extracted. Indeed, the deviation from a $\exp(-v^*/v)$ law of the data of Ref. [37] in Fig. 44 does indicate that there is a large effect from

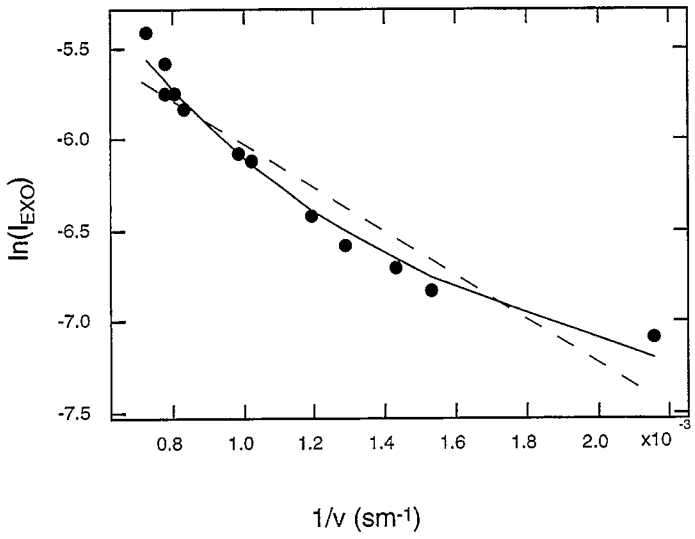

Fig. 44. Logarithm of exoemission yield in $Cl_2 + K$ reaction versus the inverse velocity of the impinging chlorine molecules from [37]. The data agree much better with the solid line, for which an additional velocity of 1.7×10^3 m/s is added to the incoming velocity than they do with the dashed line that implies no acceleration in the adsorption process.

the image acceleration as is found in the case of oxygen [30]. In fitting the Cl_2 + K data from [37] to the law

$$P_{exo} = p_0 \exp(-v^*/\alpha(v_c + v_\perp)) \tag{11}$$

a value v_c for the image acceleration induced velocity of 1.7×10^3 m/s is found, if a value p_0 of 0.2 is assumed. This is fully compatible with the energies indicated by the emission of negative ions (cf. Fig. 8). The application of the more appropriate $\exp(-v^*/\alpha(v_c + v_\perp))$ law yields of course other v^* values than the $\exp(-v^*/v_\perp)$ law. While Hellberg et al. quote a value of 1.2×10^3 m/s for v^*, the law that includes the chemical acceleration yields $v^*/\alpha = 1.2 \times 10^4$ m/s.

5. Conclusions

Aspects of molecular dynamics at surfaces that pivot on non-adiabatic consequences of charge-transfer between the reactant molecules and mostly metallic surfaces are the major focus of this study. It investigates bond-breaking, intermediate atomic motion and bond-production. The experimental probe is photons, electrons or negative ions that are emitted naturally during a reaction. The analysis of this "non-adiabatic particle emission" provides insight into the kinetics and dynamics of highly exothermic surface reactions. The content of information increases if surface properties such as the work function or the density of states at the Fermi level are varied or if the impinging molecules are prepared selectively. Two categories of exoemission are distinguished: (i) The *stimulated* emission that is driven by the release of energy from metastable structures on the surface and (ii) the *spontaneous* emission that is immediately related with the impact of the molecules on the surface. All spontaneous reactions known so far can be interpreted in the framework of a model where "harpooning" is the prerequisite for the non-adiabatic process. Harpooning, i.e. resonant ionization of the impinging molecule causes a strong acceleration of the molecular ion and may force it to leave the adiabatic potential energy surface. This partly explains negative ion emission. For electron emission a second electron transfer on the dissociating molecule has to trigger Auger emission. The "chemical hole diving" model describes the injection of a hole state localized on an adsorbing species into the Fermi sea and allows one to estimate the timescale for the reactions. Together with seeded molecular beam experiments where the velocity of the impinging molecules is varied, the velocity uptake of the non-adiabatically reacting molecules can be derived. These velocities turn out to be hyperthermal, i.e. of the order of 2×10^3 m/s and appease the interest for high "effective temperatures", i.e. kinetic energies of reaction products during their formation on surfaces.

The paper summarizes the recent improvements in the experiments and developments in theories for non-adiabatic particle emission. It shall hint the potential of the method and demonstrates that "exoemission" is effective for a contribution in the field of molecular dynamics in modern surface science.

6. Abbreviations and symbols

a_0	Bohr radius 0.529 Å
A	electropositive substrate such as for example alkali metals
α	efficiency number

α_0	fine structure constant 1/137
α_{Aug}	exponential factor for the lifetime broadening of Auger decays
A_0	pre exponential factor for the lifetime dependence
β	heating rate
b	constant
γ	energy broadening
Γ_{Auger}	Auger recombination rate
Γ_{rad}	radiative recombination rate
κ	exponent in the power law for the yield near threshold
χ_{P}	Pauling electronegativity $=\frac{1}{2}(I_{\mathrm{p}}-E_{\mathrm{A}})$
χ	image potential shift of the affinity level
D	dissociation energy
d	gas exposure $\int p\,\mathrm{d}t$
Δ_0	linewidth
E_{B}	binding energy measured from the Fermi level $(=E_{\mathrm{F}}-E)$
E_{V}	vacuum level
E_{F}	Fermi level
E_0	valence band bottom
E_x	excess energy in the vacuum measured rel. to $E_{\mathrm{V}}(=E-E_{\mathrm{V}})$
E_{A}	electron affinity measured from $E_{\mathrm{V}}(=E_{\mathrm{V}}-E)$
$E_{\mathrm{A}}^{\mathrm{A}}$	adiabatic electron affinity (cf. Fig. 3)$(=E_{\mathrm{V}}-E)$
$E_{\mathrm{A}}^{\mathrm{V}}$	vertical electron affinity (cf. Fig. 3)$(=E_{\mathrm{V}}-E)$
ε_x	excitation energy measured from $E_{\mathrm{F}}(=E_{\mathrm{F}}-E)$
ε_{A}	electron affinity measured from $E_{\mathrm{F}}(=E_{\mathrm{F}}-E)$
E'_{A}	electron affinity measured from $E_{\mathrm{V}}(=E_{\mathrm{V}}-E)$
E_{Kick}	energy transfer that is required for negative ion escape
E_{m}	kinetic energy measured rel. to $E_{\mathrm{V}}(=E-E_{\mathrm{V}})$
E_{Rydberg}	Rydberg energy 13.61 eV
E_{trans}	translational kinetic energy of molecules
ε_0	dielectric constant $8.854\times10^{-12}\,\mathrm{AsV^{-1}m^{-1}}$
e	elementary charge $1.602\times10^{-19}\,\mathrm{C}$
e^-	electron
η	efficiency
Φ	work function
$\Delta\Phi$	work function change
F_{C}	Coulomb force
$\hbar$	Planck constant/2π $6.582\times10^{-16}\,\mathrm{eVs}$
I	intensity
I_{P}	ionization potential
k_{B}	Boltzmann constant $8.617\times10^{-5}\,\mathrm{eV/K}$
$k_{i\perp}$	normal component of wave vector inside the solid
$k_{m\perp}$	normal component of wave vector outside the solid
$k_{i\parallel}$	parallel component of wave vector inside the solid
$k_{m\parallel}$	parallel component of wave vector outside the solid

l_0	typical length scale
L	Langmuir (1 L = 1 s 10^{-6} Torr)
M_{Auger}	matrix element for Auger transitions
P	power
p_0	initial probability
P_e	electron emission probability
P_{exo}	exoemission probability $P_{ion} + P_e$
P_h	probability of the existence of a hole
P_{ion}	ion emission probability
P_{photon}	photon emission probability
p	pressure
q	charge in units of the elementary charge e
Ψ_{1i}	one electron wave function of initial state 1
Ψ_{2f}	one electron wave function of final state 2
ν	frequency factor
n_v	vibrational quantum number
$S(E_m)$	kinetic energy distribution of Auger electrons inside the solid
r_S	Wigner–Seitz radius (radius of sphere containing one electron)
T_m	characteristic temperature at which a maximum is observed
t_ε	time for hole injection to excitation energy ε_A
τ_0	characteristic time constant
τ_{el}	characteristic time constant for electronic motion
τ_{nuc}	characteristic time constant for nuclear motion
τ_ε	hole lifetime at ε_A
τ_{Aug}	Auger decay time
θ_c	total reflection angle
θ	emission angle measured from the surface normal
U	inner potential $E_V - E_0$
$v_\perp$	normal velocity
v^*	characteristic velocity
X	electronegative adsorbate species
Y	Yield
Z	atomic number of element
z_{fr}	freezing distance
$z_{harpooning}$	harpooning distance (cf. Eq. (1))

Acronyms

CSEE	chemically stimulated exoelectron emission
HOMO	highest occupied molecular orbital
HREELS	high resolution electron energy loss spectroscopy
LEED	low energy electron diffraction
LSDA	local spin density approximation
LUMO	lowest unoccupied molecular orbital

MDS	metastable de-excitation spectroscopy
ML	atomic monolayer
OSEE	optically stimulated exoelectron emission
STM	scanning tunneling microscopy
TDS	thermal desorption spectroscopy
TSEE	thermally stimulated exoelectron emission
UHV	ultra high vacuum ($p < 10^{-8}$ mbar)
XPS	X-ray photoelectron spectroscopy

Acknowledgements

This paper is based on a three-year stage at the Fritz-Haber-Institut (FHI), where the author came in touch with exoemission. First of all he profited from the skills of A. Böttcher and from G. Ertl's hospitality and continuous support on all levels. The fruitful research atmosphere on the second floor of the FHI was guaranteed by D. Fick, A. Morgante, R. Grobecker, T. Gießel, S. Fichtner-Endruschat, I. Reinhardt, K. Freihube, K. Hermann, E. Piltz, G. Heyne, H. Bludau, H. Shi, R. Schuster, H. Over and K. Jacobi. I thank M. Hunt, J. Osterwalder and H. Blatter for critically proof reading the manuscript. The work was sponsored by the Alexander von Humboldt Stiftung and the Schweizerischen Nationalfonds.

References

[1] J.K. Nørskov, D.M. Newns and B.I. Lundqvist, Surf. Sci. 80 (1979) 179.
[2] H. Hertz, Ann. Phys. 31 (1887) 983.
[3] W. Hallwachs, Ann. Phys. 33 (1887) 301.
[4] P. Lennard, Ann. Phys. 8 (1902) 149.
[5] J.C. McLennan, Phil. Mag. 3 (1902) 195.
[6] A. Einstein, Ann. Phys. 17 (1905) 132.
[7] J.J. Thomson, Phil. Mag. 10 (1905) 584.
[8] F. Haber and G. Just, Ann. Phys. 30 (1909) 411.
[9] F. Haber and G. Just, Ann. Phys. 36 (1911) 308.
[10] A.K. Denisoff, Proc. R. Soc. (London) A 150 (1935) 495.
[11] F. Haber and W. Zisch, Z. Phys. 9 (1922) 302.
[12] H. Beutler and M. Polanyi, Z. Phys. 47 (1928) 379.
[13] R.A. Ogg and M. Polany, Trans. Faraday Soc. 31 (1935) 1375.
[14] J.L. Magee, J. Chem. Phys. 8 (1940) 687.
[15] W. Geiger, Z. Phys. 140 (1955) 608.
[16] W. Hanle, Acta Phys. Austricia 10 (1957) 399.
[17] J. Kramer, Z. Phys. 125 (1949) 739.
[18] J. Kramer, Z. Phys. 129 (1951) 34.
[19] F.R. Brotzen, Phys. Status Solidi 22 (1967) 9.
[20] Surface Science: The First Thirty Years (North-Holland, Amsterdam, 1994).
[21] T.F. Gesell, E.T. Arakawa and T.A. Callcott, Surf. Sci. 20 (1970) 174.
[22] J. Ferrante, ASLE Trans. 20 (1977) 328.
[23] B. Kasemo, Phys. Rev. Lett. 32 (1974) 1114.

[24] Chemical Kinetics, Physical Chemistry Series One (Butterworths, London, 1972).
[25] S.W.S. McKeever, Thermoluminescence of Solids (Cambridge University Press, Cambridge, 1985).
[26] T. Greber, R. Grobecker, A. Morgante, A. Böttcher and G. Ertl, Phys. Rev. Lett. 70 (1993) 1331.
[27] K. Hermann, K. Freihube, T. Greber, A. Böttcher, R. Grobecker, D. Fick and G. Ertl, Surf. Sci. 313 (1994) L806.
[28] R. Grobecker, H. Shi, H. Bludau, T. Hertel, T. Greber, A. Böttcher, K. Jacobi and G. Ertl, Phys. Rev. Lett. 72 (1994) 578.
[29] A. Böttcher, A. Morgante, T. Gießel, T. Greber and G. Ertl, Chem. Phys. Lett. 231 (1994) 119.
[30] T. Greber, A. Morgante, S. Fichtner-Endruschat and G. Ertl, Surf. Rev. Lett. 2 (1995) 273.
[31] A. Gross, B. Hammer, M. Scheffler and W. Brenig, Phys. Rev. Lett. 73 (1994) 3121.
[32] A. Gross, S. Wilke and M. Scheffler, Phys. Rev. Lett. 75 (1995) 2718.
[33] T. Greber, Chem. Phys. Lett. 222 (1994) 292.
[34] H. Nakatsuji, J. Chem. Phys. 87 (1987) 4995.
[35] A. Böttcher and H. Niehus, in: Proc. 11th EEEA Int. Symp. on Exoemission and its Applications, Glucholazy, Poland, 1994, p. 133.
[36] Y. Wang, J. Chem. Phys. 102 (1995) 525.
[37] L. Hellberg, J. Strömquist, B. Kasemo and B.I. Lundqvist, Phys. Rev. Lett. 74 (1995) 4742.
[38] J. Strömquist, L. Hellberg, B. Kasemo and B.I. Lundqvist, Surf. Sci. 352–354 (1996) 435.
[39] L.A. Kappers, R.L. Kroes and E.B. Hensley, Phys. Rev. B 1 (1970) 4151.
[40] V.T. Coon, Surf. Sci. 88 (1979) L42.
[41] R.F. Roose and G. Offergeld, Surf. Sci. 71 (1977) 462.
[42] I.W.M. Smith, Kinetics and Dynamics of Elementary Gas Reactions (Butterworth, London, 1980).
[43] B. Kasemo and L. Walldén, Surf. Sci. 53 (1975) 393.
[44] D. Andersson, B. Kasemo and L. Walldén, Surf. Sci. 152/153 (1984) 576.
[45] J.C. Whitehead, D.R. Hardin and R. Grice, Mol. Phys. 23 (1972) 787.
[46] P. Davidovits and D.L. McFadden, Alkali Halidi Vapors: Structure, Spectra, and Reaction Dynamics (Academic Press, New York, 1979).
[47] M.J.W. Boness and G.J. Schulz, Phys. Rev. A 2 (1970) 2182.
[48] J.K. Nørskov, Physica B 127 (1984) 183.
[49] B. Kasemo and L. Walldén, Solid State Commun. 15 (1974) 571.
[50] A. Blandin, J. Phys. Radium 22 (1961) 507.
[51] T. Greber, K. Freihube, A. Böttcher, R. Grobecker, K. Hermann, D. Fick and G. Ertl, Phys. Rev. B 50 (1994) 8755.
[52] W.L. Fite and P. Irving, J. Chem. Phys. 56 (1972) 4227.
[53] S.M. Lin, J.C. Whitehead and R. Grice, Mol. Phys. 27 (1974) 741.
[54] G.P. Reck, B.P. Mathur and W. Rothe, J. Chem. Phys. 66 (1977) 3847.
[55] L.D. Trowbridge and D.R. Hershbach, J. Vac. Sci. Technol. 18 (1984) 588.
[56] E.B. deBlasi Bourdon and R.H. Prince, Surf. Sci. 144 (1984) 591.
[57] B. Kasemo, E. Törnquist, J.K. Nørskov and B.I. Lundqvist, Surf. Sci. 89 (1979) 554.
[58] R.H. Prince and R. Persaud, Surf. Sci. 207 (1988) 207.
[59] R.H. Prince, R.M. Lambert and J.S. Foord, Surf. Sci. 107 (1981) 605.
[60] J. Hölzl and F.K. Schulte, Work Function of Metals, Springer Tracts of Modern Physics (Springer, Berlin, 1979).
[61] L. Grunberg and K.H.R. Wright, Proc. R. Soc. (London) A 232 (1955) 26.
[62] R.H. Fowler, Phys. Rev. 38 (1931) 45.
[63] P. Lange, J.K. Sass, R. Unwin and D.M. Tench, J. Electroanal. Chem. 122 (1981) 387.
[64] H.H. Rotermund, S. Jakubith, S. Kubala, A. von Oertzen and G. Ertl, J. Electron Spectrosc. Rel. Phen. 52 (1990) 811.
[65] H.D. Hagstrum, Phys. Rev. 96 (1954) 336.
[66] F.M. Propst, Phys. Rev. 129 (1963) 7.
[67] E.B. deBlasi Bourdon and R.H. Prince, Surf. Sci. 144 (1984) 581.
[68] R.H. Prince, Surf. Sci. 175 (1986) 55.
[69] G. Blaise and A. Nourtier, Surf. Sci. 90 (1979) 495.
[70] J.K. Nørskov and B.I. Lundqvist, Phys. Rev. B 19 (1979) 5661.
[71] M.L. Yu, Phys. Rev. Lett. 47 (1981) 1325.

[72] G.A. Kimmel and B.H. Cooper, Phys. Rev. B 48 (1993) 12164.
[73] P. Avouris and R.E. Walkup, Annu. Rev. Phys. Chem. 40 (1989) 173.
[74] R.D. Ramsier and J.T. Yates, Jr., Surf. Sci. Rep. 12 (1991) 243.
[75] A. Böttcher, R. Grobecker, T. Greber and G. Ertl, Chem. Phys. Lett. 208 (1993) 404.
[76] G. Hertzberg, Molecular Spectra and Molecular Structure (Van Nostrand, New York, 1945).
[77] T.L. Gilbert and A.C. Wahl, J. Chem. Phys. 55 (1971) 5247.
[78] J.W. Gadzuk, Surf. Sci. 6 (1967) 133.
[79] P. Nordlander and J.C. Tully, Surf. Sci. 211/212 (1989) 207.
[80] A. Böttcher, A. Morgante and G. Ertl, Surf. Sci. 359 (1996) L461.
[81] A. Böttcher, A. Morgante, R. Grobecker, T. Greber and G. Ertl, Phys. Rev. B 49 (1994) 10607.
[82] A. Blandin, A. Nourtier and D.W. Hone, J. Phys. (Paris) 37 (1976) 369.
[83] P. Auger, Compt. Rend. 177 (1923) 169.
[84] P.T. Landsberg, Phys. Status Solidi 41 (1970) 457.
[85] M.P. Cox, J.S. Foord, R.M. Lambert and R.H. Prince, Surf. Sci. 129 (1983) 399.
[86] W. Maus-Friedrichs, S. Dieckhoff, M. Wehrhahn, S. Plüm and V. Kempter, Surf. Sci. 271 (1992) 113.
[87] T. Fondén and A. Zwartkruis, Surf. Sci. 269/270 (1992) 601.
[88] R. Weissmann and K. Müller, Surf. Sci. Rep. 1 (1981) 251.
[89] P.T. Landsberg and M.J. Adams, J. Lumin. 7 (1973) 3.
[90] G.C. Allen, P.M. Tucker, B.E. Hayden and D.F. Klemperer, Surf. Sci. 102 (1981) 207.
[91] J. Lohff and H. Raether, Z. Phys. 142 (1955) 310.
[92] J. Lohff, Z. Phys. 146 (1956) 436.
[93] S.Z. Roginskii, in: Proc. 4th Int. Congr. on Catalysis, Moscow, 1966, p. 212.
[94] L.I. Ivankin, Fiz. Tverd. Tela 17 (1975) 1146.
[95] R.J. Breakspere and R.L. Read, Chem. Scr. 9 (1976) 116.
[96] Y.N. Rufov, A.A. Kadushin and S.Z. Roginskii, Dokl. Akad. Nauk SSSR 171 (1966) 905.
[97] M. Breyesse, B. Claudel, L. Faure and H. Latreille, Farad. Disc. 58 (1974) 205.
[98] L.E. Brus and J.J. Comas, J. Chem. Phys. 54 (1971) 2771.
[99] T.F. Gesell and E.T. Arakawa, Surf. Sci. 33 (1972) 419.
[100] B. Kasemo and E. Törnqvist, Ned. Tijdschr. Vacuumtech. 16 (1978) 37.
[101] J. Harris, B. Kasemo and E. Törnqvist, Chem. Phys. Lett. 52 (1980) 538.
[102] B. Kasemo, E. Törnqvist and L. Walldén, Mater. Sci. Eng. 42 (1980) 23.
[103] J.J. Uebbing and L.W. James, J. Appl. Phys. 41 (1970) 4505.
[104] B. Kasemo and L. Walldén, Surf. Sci. 75 (1978) L379.
[105] A. Böttcher, R. Imbeck, A. Morgante and G. Ertl, Phys. Rev. Lett. 65 (1990) 2035.
[106] B. Woratscheck, W. Sesselmann, J. Küppers and G. Ertl, Phys. Rev. Lett. 55 (1985) 611.
[107] H. Brenten, H. Müller and V. Kempter, Z. Phys. D 22 (1992) 1992.
[108] R. Hemmen and H. Conrad, Phys. Rev. Lett. 67 (1991) 1314.
[109] A. Böttcher, R. Grobecker, R. Imbeck, A. Morgante and G. Ertl, J. Chem. Phys. 95 (1991) 3756.
[110] H. Shi and K. Jacobi, Surf. Sci. 303 (1994) 67.
[111] T. Greber, A. Morgante, S. Fichtner-Endruschat and G. Ertl, in: Proc. 11th EEEA Int. Symp. on Exoemission and its Applications, Glucholazy, Poland, 1994, p. 143.
[112] A. Böttcher, T. Gießel, A. Morgante, T. Greber and G. Ertl, unpublished.
[113] H. Glaefeke, in: Thermally Stimulated Relaxation in Solids, Topics in Applied Physics 37, Ed. P. Bräunlich (Springer, Berlin, 1979).
[114] H. Brenten, H. Müller, W. Maus-Friedrichs, S. Dieckhoff and V. Kempter, Surf. Sci. 262 (1992) 151.
[115] R. Grobecker, T. Greber, A. Böttcher and G. Ertl, Phys. Status Solidi (a) 146 (1994) 119.
[116] A. Böttcher, R. Grobecker, T. Greber, A. Morgante and G. Ertl, Surf. Sci. 280 (1993) 170.
[117] H. Over, H. Bludau, M. Skottke-Klein, G. Ertl, W. Moritz and C.T. Campbell, Phys. Rev. B 45 (1992) 8659.
[118] H. Bludau, H. Over, T. Hertel, M. Gierer and G. Ertl, Surf. Sci. 342 (1995) 134.
[119] J. Trost, J. Wintterlin and G. Ertl, Surf. Sci. 329 (1995) L583.
[120] G. Ertl, Label given in a discussion at the Fritz Haber Institute in 1994.

[121] H.A. Michelsen, C.T. Rettner and D.J. Auerbach, Surface Reactions (Springer, Berlin, 1993).
[122] B. Hammer, K.W. Jacobsen and J.K. Nørskov, Phys. Rev. Lett. 69 (1992) 1971.
[123] G.P. Brivio and T.B. Grimley, Surf. Sci. 131 (1983) 475.
[124] W. Gordy and W.J.O. Thomas, J. Chem. Phys. 24 (1956) 439.
[125] S. Yamamoto, K. Susa and U. Kawabe, J. Chem. Phys. 60 (1974) 4076.
[126] D. Pines and P. Nozières, The Theory of Quantum Liquids (Benjamin, New York, 1966).
[127] H. Brune, J. Wintterlin, R.J. Behm and G. Ertl, Phys. Rev. Lett. 68 (1992) 624.
[128] J. Wintterlin, R. Schuster and G. Ertl, Phys. Rev. Lett. 77 (1996) 123.
[129] G. Wahnström, A.B. Lee and J. Strömqvist, J. Chem. Phys. 105 (1996) 326.
[130] C. Engdahl and G. Wahnström, Surf. Sci. 312 (1994) 429.
[131] D.E. Sanders and A.E. DePristo, Surf. Sci. 254 (1991) 341.
[132] J. Jacobsen, B. Hammer, K.W. Jacobsen and J.K. Nørskov, Phys. Rev. B 52 (1995) 14954.
[133] B. Kasemo, Surf. Sci. 363 (1996) 22.
[134] R. Brako and D.M. Newns, Rep. Progr. Phys. 52 (1989) 655.
[135] J. Los and J.J.C. Geerlings, Phys. Rep. 190 (1990) 133.
[136] A. Amirav, Comm. At. Mol. Phys. 24 (1990) 187.
[137] J.W. Gadzuk, Comm. At. Mol. Phys. 16 (1985) 219.
[138] P.J. Feibelman, Surf. Sci. 160 (1985) 139.
[139] J.W. Gadzuk and S. Holloway, Chem. Phys. Lett. 114 (1985) 314.
[140] S. Holloway and J.W. Gadzuk, Surf. Sci. 152 (1985) 838.
[141] A.W. Klein, J. Los and E.A. Gislason, Phys. Rep. 90 (1982) 1.